EXTENDING COHERENT EFFECTS FROM ATOMIC AND MOLECULAR MEDIA TO PLASMAS AND NANOSTRUCTURES

A Dissertation

by

DONG SUN

Submitted to the Office of Graduate Studies of
Texas A&M University
in partial fulfillment of the requirements for the degree of

DOCTOR OF PHILOSOPHY

December 2011

Major Subject: Physics

EXTENDING COHERENT EFFECTS FROM ATOMIC AND MOLECULAR MEDIA TO PLASMAS AND NANOSTRUCTURES

A Dissertation

by

DONG SUN

Submitted to the Office of Graduate Studies of
Texas A&M University
in partial fulfillment of the requirements for the degree of

DOCTOR OF PHILOSOPHY

Approved by:

Co-Chairs of Committee,	Yuri V. Rostovtsev
	Marlan O. Scully
Committee Members,	Goong Chen
	George R. Welch
	M. Suhail Zubairy
Head of Department,	Edward Fry

December 2011

Major Subject: Physics

ABSTRACT

Extending Coherent Effects from Atomic and Molecular Media to Plasmas and Nanostructures. (December 2011)

Dong Sun, B.S., Zhejiang University;

M.S., University of Antwerp

Co–Chairs of Advisory Committee: Dr. Yuri V. Rostovtsev
Dr. Marlan O. Scully

Quantum coherence and interference(QCI) effects have been studied for decades and are widely exploited in many areas. For media with QCI effect, the optical properties can change drastically, which leads to many interesting effects, such as coherent population trapping, electromagnetically induced transparency(EIT), lasing without population inversion(LWI) and so on.

We have theoretically studied the pulsed regime of EIT. In particular, simulations of propagation of gaussian and $0-\pi$ co-propagating laser pulses in a medium consisting of 3-level Λ-atoms have been performed. It has been found that, even at the two-photon resonance, the length of propagation for the $0-\pi$ pulses is much smaller than that for the Gaussian probe pulses. We explained such a behavior using the dark and bright basis and the dressed state basis. Some possible applications are discussed.

We also investigated the collision-induced coherence of two decay channels along two optical transitions. Quantum interference will suppress the spontaneous emission. The degree of this suppression is measured by the branch ratio of these two transitions. Our preliminary calculations show that a significant decrease of the branching ratio with increase of electron densities is reproduced in the theory.

We have developed a new variant of Raman spectroscopy with shaped femtosecond pulses. It has several advantages to be applied in multiscatterd media. It is based on change of the spectra of femtopulses due to Raman scattering (stimulated or coherent). The technique can be used for a broad range of applications from atomic and molecular optical and IR spectroscopy to spore detection and tissue microscopy.

Finally, we have shown that Fano interference in the decay channels of three levels system can lead to considerably different absorption and emission profiles. We found that a coherence can be built up in the ground state doublet whose strength depends on a coupling parameter that arises from Fano interference. This can in principle lead to breaking of the detail balance between the absorption and emission processes in atomic systems.

To my parents Qiwu Sun and Xiuhua Jia, my wife Jingqiong

ACKNOWLEDGMENTS

First of all, I would like to thank my advisors Dr. Yuri Rostovtsev and Dr. Marlan Scully for all the time they have spent with me and all their patience, advice, and support during my research. I could not have made it without their help.

I am very grateful to all my the committee members, Dr. Goong Chen, Dr. George Welch and Dr. Zubairy, for their valuable time and guidance during my study and research.

Special thanks to Dr. Sumanta Das and Dr. Zoe-Elizabeth Sariyanni for their wonderful joint work, discussions, and continuous help in my research.

Many thanks to Dr.Hebin Li, Dr. Jiahui Peng, Dr. Xi Wang, Dr. Qingqing Sun, Dr. Konstantin E. Dorfman, Eyob Sete, Dr. Miaochan Zhi, Dongxia Ma, Kai Wang, Anatoly Svidzinsky, and Dr. Alexei Sokolov, for sharing their knowledge and experience with me, making my time at Texas A&M a wonderful experience.

Thanks to the physics department and the Robert A. Welch Foundation (Grant No. A-1261) for the financial support of my research.

Many thanks to Ms. Kimberly Chapin, Mr. Clayton Holle, and Ms. Sandi Smith for their cheerful help and support in the past years. It has been a great pleasure to work with them.

Finally, I would like to thank my whole family for their forever support and encouragement.

TABLE OF CONTENTS

CHAPTER Page

LIST OF FIGURES

FIGURE Page

FIGURE Page

CHAPTER I

INTRODUCTION TO COHERENT EFFECTS

Quantum coherence effects, such as Coherent Population Trapping (CPT) [1] and Electromagnetically Induced Transparency (EIT)[2, 3, 4, 5], have been the focus of broad research activities for the last two decades, as they drastically change optical properties of media. For example, for EIT in CW and pulsed regimes [3, 4, 5, 6, 7], absorption practically vanishes. Media with excited coherence may display high index of refraction without absorption [8]. The corresponding steep dispersion results in the ultra-slow or fast propagation of light pulses [9, 10, 11, 12, 13] which can produce huge optical delays [13]. This dispersion can be used for drastic modification of the phase-matching conditions for Brillouin scattering [14], four-wave mixing [15], controlable switching between bunching and anti-bunching [16], phase effects in EIT [17] dark state polariton [18], storage and retrieval of pulses [19], and freezing of a light pulse[20]. EIT has led to several other coherent phenomena like enhancing the sensitivity of magnetometry [21, 22], dynamical control[23, 24], single atom cavity QED [25] and optical switch[26, 27, 28, 29]. It is possible to achieve manipulation of a coherent medium, optical pulses faster than the relaxation rates [30] and enhanced nonlinear effects at a few photon level [31, 32]; and to develop a bright source for efficient generation of far IR pulses [33, 34].

EIT has been achieved in atomic [2, 3, 5] and molecular [35, 36] gases, BEC [9], solid state systems [37, 38, 39], meta-materials [40, 41, 42], and even in mechanical effect of light [43]. Physics of coherent effects in Λ-type three-level atoms is related to excitation of the maximum coherence between two ground states (in alkali atoms,

---

The journal model is Physics Review A.

these are the hyperfine levels) under the condition when a special coherent state, the so-called dark state, is formed.

In the past few decades the study of quantum interference and coherence effects in atomic and molecular systems [44] has led to numerous fascinating phenomena, e.g., Fano interferences [45], vacuum induced coherence [46], lasing without inversion [47, 48], quantum Carnot engine [49] and long lived coherences in biochemical molecules [50].

The application of coherence in solar energy physics in fact can change the balance processes that are limiting the operation of quantum systems [51]. For example, for a quantum photocell, the fundamental limit to the efficiency is accepted to be in the balance of radiative absorption and recombination. The coherence effects can in fact break this balance and significantly suppress the emission process which will result in enhancement of the power generated by photo-cell. One of the possible ways to break the balance between recombination and absorption is via the coherent drive similar to the LWI process [52, 53], where the coherence between two levels induced by external source [54] can cancel the emission processes. It is also possible to generate the coherence without use of external field. This approach is based on Fano effect [55] which manifests itself as an interference between the eigenstates of the system. For example, Fano interference was obtained between states of two coupled quantum wells via tunneling [56]. The direct application in an optical system by means of laser without inversion resonances was analyzed in [53] and has the name Fano-Harris lasing without inversion to distinguish it from the standard (externally driven) lasing without inversion. The latest results showed that quantum coherence that arise from quantum noise via Fano coupling can significantly enhance the efficiency of the solar cell up to the Carnot limit [57]. In the latter work, a three level system with Fano-coupled doublet in the ground state that decays to identical continuum of levels

demonstrates the enhancement in efficiency, but the effect of interference between discrete system of the levels and continuum reservoir was not studied properly.

In this dissertation we discuss the effects of atomic coherence and interference in several different systems. This dissertation is organized as follows: Chapter II studies the effect of laser pulse shape on EIT; Chapter III studies the nonlinear spectroscopy with $0-\pi$ pulses in molecular systems; Chapter IV studies the quenching of spontaneous emission in plasmas and branch ratio of multilevel system; Chapter V studies the coherent effect of fano interference on photovoltaics in nanostructure; and Chapter VI summarizes the results of our work.

In our work, interaction of electromagnetic radiation with matter described by the semiclassical theory and the effects of light propagation in medium play important roles in the studies of coherent effects. We will first give a simple introduction to these parts.

A. Semiclassical theory

Semiclassical theory is widely used to extract the properties of atom-field interaction, in which the field is treated as classical electromagnetic field, while the atoms are considered as quantum system. One classical example involving the atom-field interaction is a single mode field interacting with a two-level atom.

We can approach this problem through either probability amplitude method or density matrix method. Consider a two-level atomic system interacting with a incident light, as shown in Fig. 1, where $|a\rangle$ and $|b\rangle$ represent the excited and the ground states, and ν is the light frequency. Ω is the Rabi frequency of incident light and $\omega_{a,b}$ is the corresponding eigenvalues of states a, b.

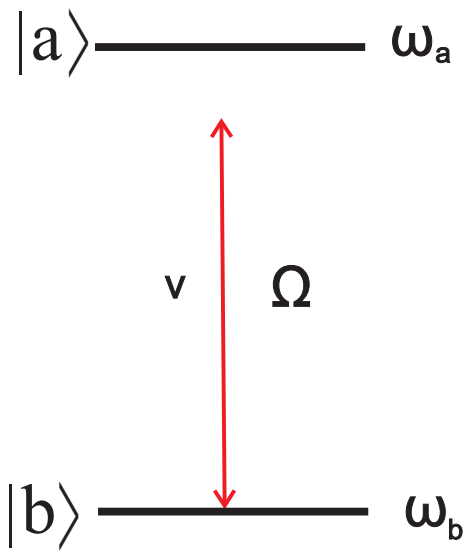

Fig. 1. Spectral picture of hole filling. Spectral components of both pulses create coherence and then the new frequency component of Ω_2 is generated to fill in the hole in the spectrum.

In the rotating-wave approximation(RWA), the system Hamiltonian is,

$$\hat{H} = \hat{H}_0 + \hat{H}_{int} \tag{1.1}$$

where

$$\hat{H}_0 = \hbar\omega_a|a\rangle\langle a| + \hbar\omega_b|b\rangle\langle b| \tag{1.2}$$

$$\hat{H}_{int} = -\frac{\hbar}{2}\left(\Omega^* e^{i\nu_1 t}|a\rangle\langle b| + H.C.\right) \tag{1.3}$$

represent the unperturbed and the interaction part of the Hamiltonian respectively.

$$\nu = \omega_a - \omega_b - \Delta \tag{1.4}$$

is the frequency of the applied pulses. Ω is the Rabi frequency and it is defined by $\Omega = \wp_{ab}E/\hbar$. in which $\wp_{ab} = e\langle a|x|b\rangle$ is the matrix element of the electric dipole

moment. The wave function of the two-level atom can be written in the form

$$|\varphi\rangle = ae^{-i\omega_a t}|a\rangle + be^{-i\omega_b t}|b\rangle \tag{1.5}$$

The evolution of the state vector obeys the Schrödinger equation

$$\frac{d}{dt}|\varphi\rangle = -\frac{i}{\hbar}\hat{H}|\varphi\rangle \tag{1.6}$$

Thus we can derive the equations of motion for the probability amplitudes of a,b, which are

$$\dot{a} = \frac{i}{2}\Omega b e^{-i\Delta t} \tag{1.7}$$

$$\dot{b} = \frac{i}{2}\Omega^* a e^{i\Delta t} \tag{1.8}$$

With a given electrical field, we can then derive the time dependency of probability amplitudes.

However, this approach is not complete. Within the probability amplitude frame, it is impossible to include terms like spontaneous decay and incoherent pumping. Now we will recalculate the evolution of this system with the density matrix method. In this case, the evolution of density matrix elements will obey the Liouville equation of motion, given by

$$\dot{\rho} = -\frac{i}{\hbar}[H_{int}, \rho] \tag{1.9}$$

which is more general than the Schrödinger equation. Then we can add phenomenological decay terms to the density operator equation Eq.1.9, give by

$$L\rho = -\frac{\gamma}{2}[\sigma^+\sigma\rho + \rho\sigma^+\sigma - 2\sigma\rho\sigma^+]; \tag{1.10}$$

where $\sigma = |b\rangle\langle a|$ is the atomic transition operator and γ is the spontaneous decay rate, and the dynamical equation of ijth element of density matrix is

$$\dot{\rho_{ij}} = -\frac{i}{\hbar}\sum_k (H_{ik}\rho_{kj} - \rho_{ik}H_{kj}) - (L\rho)_{ij} \tag{1.11}$$

thus we get the dynamical equations of density matrix

$$\dot{\rho_{bb}} = i\Omega^*\rho_{ab} - i\Omega\rho_{ba} + \gamma\rho_{aa} \tag{1.12}$$

$$\dot{\rho_{ab}} = -\Gamma_{ab}\rho_{ab} + i\Omega^*(\rho_{aa} - \rho_{bb}) - i\Omega^*\rho_{ab} \tag{1.13}$$

where

$$\Gamma_{ab} = \frac{\gamma}{2} + i\Delta \tag{1.14}$$

with the condition

$$\rho_{aa} + \rho_{bb} = 1 \tag{1.15}$$

for closed system.

B. Propagation of electromagnetic wave

When laser pulses pass through an optically thick medium such as a solid state resonant medium, there are pulse-medium interactions between them and these interactions are position dependent. The incident pulses will not only introduce coherence in the resonant medium, but also create dipole moments. These dipole moments at different positions will gradually affect the properties of pulses, such as the pulse intensity and spectrum. If the medium is thick enough, the modification of pulses can not be ignored. A self-consistent theory taking into consideration the effect of both the field and the atoms is needed to calculate the evolution of the system.

It is known that the propagation of laser pulses(electromagnetic wave in special range) is ruled by Maxwell's Equation. Consider the situation in a completely empty

region of space, where there is no charge. We can write Maxwell's Equations as

$$\nabla \cdot \mathbf{E} = 0 \tag{1.16}$$

$$\nabla \times \mathbf{B} = 0 \tag{1.17}$$

$$\nabla \times \mathbf{B} - \frac{1}{c}\frac{\partial \mathbf{E}}{\partial t} = \frac{4\pi}{c}\mathbf{J} \tag{1.18}$$

$$\nabla \times \mathbf{E} + \frac{1}{c}\frac{\partial \mathbf{B}}{\partial t} = 0 \tag{1.19}$$

where c is the speed of light and J is the current density.

Taking the curl of the last equation, and using the vector identity $\nabla \times (\nabla \times \mathbf{E}) = \nabla(\nabla \cdot \mathbf{E}) - \nabla^2\mathbf{E}$, we obtain

$$\frac{\partial^2 E(z,t)}{\partial z^2} - \frac{1}{c^2}\frac{\partial^2 E(z,t)}{\partial t^2} = \frac{4\pi^2}{c^2}\frac{\partial^2 P}{\partial t^2} = -\frac{4\pi^2}{c^2}\nu^2 P \tag{1.20}$$

where P is the polarization and is given by

$$J = \frac{\partial P}{\partial t} \tag{1.21}$$

The electrical field can be rewritten as

$$E(z,t) = \mathcal{E}(z,t)e^{-i\nu t + ikz} \tag{1.22}$$

therefore

$$\frac{\partial E(z,t)}{\partial z} = \frac{\partial \mathcal{E}(z,t)}{\partial z}e^{-i\nu t + ikz} + ik\mathcal{E}(z,t)e^{-i\nu t + ikz} \tag{1.23}$$

thus we can get

$$\frac{\partial^2 E(z,t)}{\partial z^2} = \frac{\partial^2 \mathcal{E}(z,t)}{\partial z^2} e^{-i\nu t+ikz} + 2ik\frac{\partial \mathcal{E}(z,t)}{\partial z} e^{-i\nu t+ikz} - k^2 \mathcal{E}(z,t) e^{-i\nu t+ikz} \tag{1.24}$$

$$\frac{1}{c^2}\frac{\partial^2 E(z,t)}{\partial t^2} = \frac{1}{c^2}\frac{\partial^2 \mathcal{E}(z,t)}{\partial t^2} e^{-i\nu t+ikz} - \frac{2i\nu}{c^2}\frac{\partial \mathcal{E}(z,t)}{\partial t} e^{-i\nu t+ikz} - \frac{\nu^2}{c^2}\mathcal{E}(z,t) e^{-i\nu t+ikz} \tag{1.25}$$

with the relation

$$k = \frac{\nu}{c} \tag{1.26}$$

and the slow varying amplitude approximation(SVAA),

$$\left|\frac{1}{\mathcal{E}}\frac{\partial \mathcal{E}(z,t)}{\partial z}\right| \ll k \tag{1.27}$$

we can ignore the first terms on the right in Eq.(1.24,1.25) and subtract Eq.(1.25) from Eq. (1.24) to arrive at

$$\frac{\partial \mathcal{E}(z,t)}{\partial z} + \frac{1}{c}\frac{\partial \mathcal{E}(z,t)}{\partial t} = 2\pi i k N \wp_{ab}\rho_{ab} \tag{1.28}$$

where N is the density of population and the relationship

$$P = N\wp_{ab}\rho_{ab} e^{-i\nu t+ikz} \tag{1.29}$$

has been exploited. $\wp_{ab}$ is the dipole moments between the levels a and b, with which the laser pulse is in resonance and ρ_{ab} is the coupling of a and b.

We can go further to the retard time frame. In the following general coordinate transformation,

$$z = a_{11}z' + a_{12}t' \tag{1.30a}$$

$$t = a_{21}z' + a_{22}t' \tag{1.30b}$$

we require that $a_{21}a_{12} \neq a_{11}a_{22}$, and the corresponding inverse transformation will be

$$z' = \frac{a_{22}z - a_{12}t}{a_{11}a_{22} - a_{21}a_{12}} \tag{1.31a}$$

$$t' = \frac{a_{21}z - a_{11}t}{a_{21}a_{12} - a_{11}a_{22}} \tag{1.31b}$$

then we can get

$$\begin{aligned}\frac{\partial \mathcal{E}(z,t)}{\partial z} &= \frac{\partial \mathcal{E}(z',t')}{\partial z'}\frac{\partial z'}{\partial z} + \frac{\partial \mathcal{E}(z',t')}{\partial t'}\frac{\partial t'}{\partial z} \\ &= \frac{\partial \mathcal{E}(z',t')}{\partial z'}\left(\frac{a_{22}}{a_{11}a_{22} - a_{21}a_{12}}\right) + \frac{\partial \mathcal{E}(z',t')}{\partial t'}\left(\frac{a_{21}}{a_{21}a_{12} - a_{11}a_{22}}\right)\end{aligned} \tag{1.32}$$

$$\begin{aligned}\frac{1}{c}\frac{\partial \mathcal{E}(z,t)}{\partial t} &= \frac{1}{c}\frac{\partial \mathcal{E}(z',t')}{\partial z'}\frac{\partial z'}{\partial t} + \frac{1}{c}\frac{\partial \mathcal{E}(z',t')}{\partial t'}\frac{\partial t'}{\partial t} \\ &= \frac{1}{c}\frac{\partial \mathcal{E}(z',t')}{\partial z'}\left(-\frac{a_{12}}{a_{11}a_{22} - a_{21}a_{12}}\right) + \frac{1}{c}\frac{\partial \mathcal{E}(z',t')}{\partial t'}\left(-\frac{a_{11}}{a_{21}a_{12} - a_{11}a_{22}}\right)\end{aligned} \tag{1.33}$$

In our case, take the following value,

$$a_{11} = 1, a_{12} = 0, a_{22} = 1, a_{21} = \frac{1}{c} \tag{1.34}$$

which is corresponding to the transformation of

$$z = z', t = \frac{z'}{c} + t' \tag{1.35}$$

and add Eq.(1.32) and Eq.(1.33) together, we will get

$$\frac{\partial \mathcal{E}(z,t)}{\partial z} + \frac{1}{c}\frac{\partial \mathcal{E}(z,t)}{\partial t} = \frac{\partial \mathcal{E}(z',t')}{\partial z'} \tag{1.36}$$

thus we will have

$$\frac{\partial \mathcal{E}(z,t)}{\partial z'} = 2\pi i k N \wp_{ab}\rho_{ab} \tag{1.37}$$

The Rabi frequency is defined as

$$\Omega = \frac{\wp_{ab}\mathcal{E}}{\hbar} \tag{1.38}$$

Therefore,

$$\frac{\partial \Omega}{\partial z'} = \frac{2\pi i k N \wp_{ab}^2 \rho_{ab}}{\hbar} = i\eta\rho_{ab} \tag{1.39}$$

where

$$\eta = \frac{2\pi i k N \wp_{ab}^2}{\hbar} \tag{1.40}$$

is the corresponding coupling constant.

CHAPTER II

EFFECT OF LASER PULSE SHAPE ON EIT*

A. Introduction

In general, the EIT has been studied in three-level Λ-type atomic systems, where a strong drive field and a weak probe field on adjacent transitions have been applied, and the fields typically have co-propagating geometry to eliminate the Doppler effect [58]. However, the effects of laser pulses having arbitrary time dependence on the EIT have not yet been addressed.

Meanwhile, it is well-known that the shape of optical pulses plays an important role in their propagation through a medium of two-level atoms. The propagation of the $2n\pi$ pulses in a two-level medium is a good example [59]. Short optical pulses with area given by

$$\theta = \int_{-\infty}^{\infty} \Omega(t')dt' = 2\pi n, \tag{2.1}$$

can propagate through an atomic gas at the resonant frequency without absorption, where $\Omega = \wp\varepsilon/\hbar$ is the Rabi frequency of applied optical pulse, $\wp$ is the dipole moments of the corresponding transition and ε is the electric field of pulse. Even weak optical pulses with pulse area equal to zero($n = 0$), the so called $0 - \pi$ pulses, have large propagation lengths. An interesting question arising in this regard is whether the propagation of pulses in EIT-configuration can be improved by using the $0 - \pi$ pulses. In this chapter, we study these effects in detail. Employing the

* Reprinted with permission from "Propagation of 0π pulses in a gas of three-level atoms" by D. Sun, Z. E. Sariyanni, S. Das, and Y. V. Rostovtsev, 2011. Phys. Rev. A, vol. 83, pp. 063815 ,Copyright[2011] by the American Physical Society.

dressed state basis, we show the mechanism of the pulse shape on EIT, and perform simulation to support the theoretical results.

Our results may find application as a method of coherent control of pulse propagation. Another interesting result is related to the spectrum change of the probe pulse during propagation through the EIT medium. The various frequencies of the probe pulse propagating through a EIT medium are influenced differently by nonlinear interaction resulting in strong modification of the pulse spectrum. We study the effect by using the $0-\pi$ pulse for this purpose. The $0-\pi$ pulse has a spectral hole that disappears while the $0-\pi$ pulse propagating through the medium due to nonlinear interaction.

The organization of this chapter is as follows. In Section II, we introduce a Λ-type 3-level system. In Section III, we simulate the effect of pulse shape on EIT, and the possible control of pulse propagation through a 3-level Λ-type medium. In section IV, we discuss possible applications. Finally in Section V we conclude by summarizing our results and give some future perspectives.

B. Model

We consider an isotropic homogeneous, medium consisting of three-level atoms in a Λ configuration. This system is driven by two co-propagating laser pulses as shown in Fig. 2. $r_{b,c}$ is the incoherent pumping rate, and $\gamma_{b,c}$ is the spontaneous decay rate from $|a\rangle$ to lower levels. The system is closed, so there is no decay or incoherent pumping outside these levels.

Note that the drive field has a frequency resonant with the transition between atomic levels $|a\rangle$ and $|c\rangle$, while the probe field has a frequency detuning Δ from the resonance. The two-photon resonance condition important for EIT can be achieved

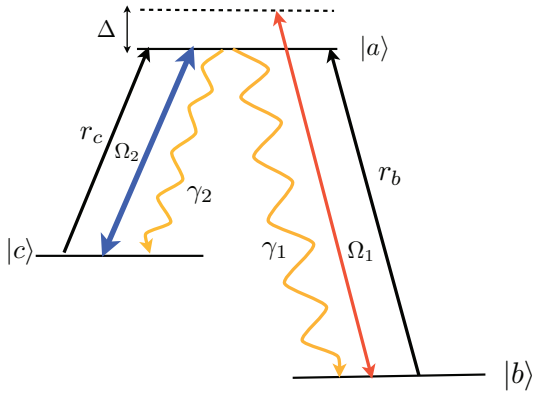

Fig. 2. Scheme of Λ-type system for EIT. The system is driven by two classical fields and incoherent pumping. The pump field has resonant frequency while probe field has a detuning Δ from the atomic resonance.

simply by tuning the probe field to the resonance ($\Delta = 0$). Level $|b\rangle$ and $|c\rangle$ are states that have lifetime longer than the pulse duration. Level $|a\rangle$ is an electronic excited state that is coupled to level $|b\rangle$ through the probe field and to level $|c\rangle$ through the drive field. Note that the transition between level $|b\rangle$ and $|c\rangle$ is dipole forbidden. In experimental schemes, the states $|b\rangle$ and $|c\rangle$ can be the hyperfine states $5S_{1/2}(F = 1)$ and $5S_{1/2}(F = 2)$ of ^{87}Rb respectively. Then the $|a\rangle$ is the $5P_{1/2}(F = 2)$.

In the rotating-wave approximation, the semiclassical time-dependent interaction Hamiltonian that describes the atom-laser coupling for this Λ system is given [2] by

$$H_{int} = -\hbar\left(\Omega_1|a\rangle\langle b| + \Omega_2|a\rangle\langle c| - \Delta|a\rangle\langle a| - \Delta|c\rangle\langle c| + H.C.\right); \tag{2.2}$$

where $\Omega_1 = \wp_{ab}\varepsilon_1/\hbar$ and $\Omega_2 = \wp_{ac}\varepsilon_2/\hbar$ is the Rabi frequency of probe (drive) field, $\wp_{ab}(\wp_{ac})$ are the dipole moments of the transition $|a\rangle \leftrightarrow |b\rangle$ ($|a\rangle \leftrightarrow |c\rangle$) and $\varepsilon_{1,2}$ are the applied electric fields of probe and pump pulse respectively.

The time evolution of the density matrix is given by the master equation [2]

$$\dot{\rho} = -\frac{i}{\hbar}[H_{int}, \rho] + L\rho; \tag{2.3}$$

where $L\rho = L_1\rho + L_2\rho + L_3\rho + L_4\rho$ describes spontaneous emission and incoherent pumping, and is given by

$$L_1\rho = -\frac{\gamma_1}{2}[\sigma_1^+\sigma_1\rho + \rho\sigma_1^+\sigma_1 - 2\sigma_1\rho\sigma_1^+], \tag{2.4}$$

$$L_2\rho = -\frac{\gamma_2}{2}[\sigma_2^+\sigma_2\rho + \rho\sigma_2^+\sigma_2 - 2\sigma_2\rho\sigma_2^+], \tag{2.5}$$

$$L_3\rho = -\frac{r_b}{2}[\sigma_1\sigma_1^+\rho + \rho\sigma_1\sigma_1^+ - 2\sigma_1^+\rho\sigma_1], \tag{2.6}$$

$$L_4\rho = -\frac{r_c}{2}[\sigma_2\sigma_2^+\rho + \rho\sigma_2\sigma_2^+ - 2\sigma_2^+\rho\sigma_2]. \tag{2.7}$$

Here $\sigma_1 = |b\rangle\langle a|$, $\sigma_2 = |c\rangle\langle a|$ are the atomic transition operators.

The dynamical evolution of the density matrix elements is given by,

$$\dot{\rho}_{bb} = i\Omega_1^*\rho_{ab} - i\Omega_1\rho_{ba} + \gamma_b\rho_{aa} - r_b\rho_{bb} \tag{2.8}$$

$$\dot{\rho}_{cc} = i\Omega_2^*\rho_{ac} - i\Omega_2\rho_{ca} + \gamma_c\rho_{aa} - r_c\rho_{cc} \tag{2.9}$$

$$\dot{\rho}_{ab} = -\Gamma_{ab}\rho_{ab} + i\Omega_1(\rho_{bb} - \rho_{aa}) + i\Omega_2\rho_{cb} \tag{2.10}$$

$$\dot{\rho}_{ca} = -\Gamma_{ca}\rho_{ca} + i\Omega_2^*(\rho_{aa} - \rho_{cc}) - i\Omega_1^*\rho_{cb} \tag{2.11}$$

$$\dot{\rho}_{cb} = -\Gamma_{cb}\rho_{cb} - i\Omega_1\rho_{ca} + i\Omega_2^*\rho_{ab} \tag{2.12}$$

where

$$\Gamma_{ab} = \frac{\gamma_1 + \gamma_2 + r_b}{2} - i\Delta \equiv \gamma_{ab} - i\Delta \tag{2.13}$$

$$\Gamma_{ca} = \frac{\gamma_1 + \gamma_2 + r_c}{2} \equiv \gamma_{ac} \tag{2.14}$$

$$\Gamma_{cb} = \frac{r_b + r_c}{2} - i\Delta \equiv \gamma_{cb} - i\Delta \tag{2.15}$$

are the complex dephasing, and the condition for close system is given by $\rho_{aa} + \rho_{bb} +$

$\rho_{cc} = 1$.

1. Basis of dark and bright states

To understand the effect of different pulse time-dependence on EIT, we can take advantage of the so-called dark and bright state basis. To simplify our calculation, we consider two-photon resonance and the Rabi frequency to be real. The interaction Hamiltonian for the Λ system can be written as

$$H_{int} = -\hbar \begin{pmatrix} 0 & \Omega_1 & \Omega_2 \\ \Omega_1 & 0 & 0 \\ \Omega_2 & 0 & 0 \end{pmatrix} \tag{2.16}$$

The state vector in this bare basis is

$$|\psi\rangle = a|a\rangle + b|b\rangle + c|c\rangle, \tag{2.17}$$

where a, b, and c are the probability amplitudes. Let u represent these amplitudes

$$u = \begin{pmatrix} a \\ b \\ c \end{pmatrix} \tag{2.18}$$

The evolution of state vector obeys the Schrödinger equation

$$|\dot{\psi}\rangle = -\frac{i}{\hbar}\hat{H}_{int}|\psi\rangle. \tag{2.19}$$

Thus the equations of motion for the amplitudes becomes

$$\dot{u} = -\frac{i}{\hbar}H_{int}u \tag{2.20}$$

which is

$$\begin{pmatrix} \dot{a} \\ \dot{b} \\ \dot{c} \end{pmatrix} = -i \begin{pmatrix} \Omega_1 b + \Omega_2 c \\ \Omega_1 a \\ \Omega_2 a \end{pmatrix} \tag{2.21}$$

Now we introduce a new basis that involves the so-called dark and bright states, namely, the bright state

$$|B\rangle = \frac{\Omega_1|b\rangle + \Omega_2|c\rangle}{\sqrt{\Omega_1^2 + \Omega_2^2}}, \tag{2.22}$$

and the dark state

$$|D\rangle = \frac{-\Omega_2|b\rangle + \Omega_1|c\rangle}{\sqrt{\Omega_1^2 + \Omega_2^2}}. \tag{2.23}$$

In this basis, the state vector is

$$|\psi\rangle = a|a\rangle + B|B\rangle + D|D\rangle, \tag{2.24}$$

Rewriting the linear relationship between these two bases in matrix form, we obtain

$$\begin{pmatrix} |a\rangle \\ |B\rangle \\ |D\rangle \end{pmatrix} = S \begin{pmatrix} |a\rangle \\ |b\rangle \\ |c\rangle \end{pmatrix}, \tag{2.25}$$

where

$$S = \begin{pmatrix} 1 & 0 & 0 \\ 0 & \frac{\Omega_1}{\Omega} & \frac{\Omega_2}{\Omega} \\ 0 & -\frac{\Omega_2}{\Omega} & \frac{\Omega_1}{\Omega} \end{pmatrix} \tag{2.26}$$

is the rotation matrix, and $\Omega = \sqrt{\Omega_1^2 + \Omega_2^2}$.

Let v represent the probability amplitudes of new basis

$$v = \begin{pmatrix} a \\ B \\ D \end{pmatrix} \tag{2.27}$$

We obtain

$$v = (S^T)^{-1}u = Su \tag{2.28}$$

or

$$u = S^{-1}v, \tag{2.29}$$

where S^T is the transposed matrix of S.

After straightforward calculations, replacing u by v in Eq. (2.20), and taking into consideration that Ω_i are function of time, we obtain

$$\dot{v} = -\frac{i}{\hbar}H_{eff}v \tag{2.30}$$

where

$$H_{eff} = SH_{int}S^{-1} - iS\dot{S}^{-1} \tag{2.31}$$

is the effective interaction Hamiltonian in the new basis. Substituting Eqs.(2.16,2.26) into Eq.(2.31), we obtain

$$H_{eff} = -\hbar \begin{pmatrix} 0 & \Omega & 0 \\ \Omega & 0 & 0 \\ 0 & 0 & 0 \end{pmatrix} - i\hbar \begin{pmatrix} 0 & 0 & 0 \\ 0 & 0 & \Omega_c \\ 0 & -\Omega_c & 0 \end{pmatrix} \tag{2.32}$$

Now it is clear that Ω is the effective Rabi frequency of coupling between the bright state, $|B\rangle$, and state $|a\rangle$, and

$$\Omega_c = \frac{\dot{\Omega}_1\Omega_2 - \dot{\Omega}_2\Omega_1}{\Omega^2} \tag{2.33}$$

is the the Rabi frequency of coupling between the dark and bright states.

Thus the Λ-system as shown in Fig. 2 becomes the effective system shown in Fig. 3, where

$$\gamma = \frac{\Omega_1^2\gamma_b + \Omega_2^2\gamma_c}{\Omega^2} \tag{2.34}$$

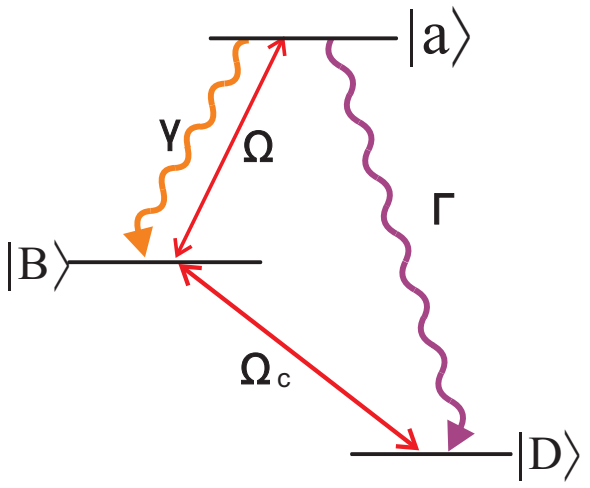

Fig. 3. Effective scheme in the dark-bright basis.

$$\Gamma = \frac{\Omega_2^2\gamma_b + \Omega_1^2\gamma_c}{\Omega^2} \tag{2.35}$$

are the effective decay rates from $|a\rangle$ to the bright and dark states correspondingly.

It can be seen that when the Rabi frequencies Ω_1 and Ω_2 have the same time dependence (i.e., the drive and probe fields are matched pulses), the Rabi frequency Ω_c is zero. There is no interaction between the bright and dark states; the effective system can be viewed as a two-level system. Once all population is trapped in the dark state, there is no absorption or excitation; this is the CPT phenomenon. On the other hand, when the probe and drive pulses have different time-dependence, there is coupling between dark and bright states that leads to absorption of probe beam and excitation of level $|a\rangle$.

2. Basis of dialogized Hamiltonian

A simple physical picture can be gained in an alternative basis of the so-called dressed states that can be obtained by diagonalizing the interaction Hamiltonian. The transformation matrices between the bare state basis and the dressed state basis are given

by

$$P^{-1} = \begin{pmatrix} 0 & \frac{1}{\sqrt{2}} & \frac{1}{\sqrt{2}} \\ \frac{\Omega_2}{\Omega} & \frac{\Omega_1}{\sqrt{2}\Omega} & -\frac{\Omega_1}{\sqrt{2}\Omega} \\ -\frac{\Omega_1}{\Omega} & \frac{\Omega_2}{\sqrt{2}\Omega} & -\frac{\Omega_2}{\sqrt{2}\Omega} \end{pmatrix}, \tag{2.36}$$

$$P = \begin{pmatrix} 0 & \frac{\Omega_2}{\Omega} & -\frac{\Omega_1}{\Omega} \\ \frac{1}{\sqrt{2}} & \frac{\Omega_1}{\sqrt{2}\Omega} & \frac{\Omega_2}{\sqrt{2}\Omega} \\ \frac{1}{\sqrt{2}} & -\frac{\Omega_1}{\sqrt{2}\Omega} & -\frac{\Omega_2}{\sqrt{2}\Omega} \end{pmatrix}, \tag{2.37}$$

The dressed states are given by

$$\begin{pmatrix} |\varphi_0\rangle \\ |\varphi_+\rangle \\ |\varphi_-\rangle \end{pmatrix} = P \begin{pmatrix} |a\rangle \\ |b\rangle \\ |c\rangle \end{pmatrix} = \begin{pmatrix} \frac{\Omega_2}{\Omega}|b\rangle - \frac{\Omega_1}{\Omega}|c\rangle \\ \frac{1}{\sqrt{2}}|a\rangle + \frac{\Omega_1}{\sqrt{2}\Omega}|b\rangle + \frac{\Omega_2}{\sqrt{2}\Omega}|c\rangle \\ \frac{1}{\sqrt{2}}|a\rangle - \frac{\Omega_1}{\sqrt{2}\Omega}|b\rangle - \frac{\Omega_2}{\sqrt{2}\Omega}|c\rangle \end{pmatrix} \tag{2.38}$$

and the state vector is

$$|\psi\rangle = \varphi_0|\varphi_0\rangle + \varphi_+|\varphi_+\rangle + \varphi_-|\varphi_-\rangle. \tag{2.39}$$

Let w represent the amplitudes in the dressed state basis

$$w = \begin{pmatrix} \varphi_0 \\ \varphi_+ \\ \varphi_- \end{pmatrix}, \tag{2.40}$$

then, we have

$$w = Pu \text{ or } u = P^{-1}w. \tag{2.41}$$

The evolution of the state vector obeys the same Schrödinger equation. Similarly, replacing u in Eq. (2.20) by w, and taking into consideration of the time dependence

of the Rabi frequency, we obtain

$$\dot{w} = -\frac{i}{\hbar} H'_{eff} w, \tag{2.42}$$

where

$$H'_{eff} = P H_{int} P^{-1} - i P \dot{P}^{-1} \tag{2.43}$$

is the effective interaction Hamiltonian in the new basis. We obtain

$$H'_{eff} = \hbar \begin{pmatrix} 0 & 0 & 0 \\ 0 & \Omega & 0 \\ 0 & 0 & -\Omega \end{pmatrix} - \frac{i}{\sqrt{2}} \hbar \begin{pmatrix} 0 & \Omega_c & -\Omega_c \\ -\Omega_c & 0 & 0 \\ \Omega_c & 0 & 0 \end{pmatrix} \tag{2.44}$$

where Ω_c is the Rabi frequency between these dressed states, the same as in Eq.(2.33).

It can be seen that when the Rabi frequencies are independent on time or the drive and probe fields are matched pulses, the second term in Eq. (2.44) is zero, and there is no coupling between the dressed states. These two basis give us different forms of the effective Hamiltonian that both lead us to the same conclusion: the different time dependence of drive and probe pulses introduces interaction between the dark and bright states and between the dressed states.

3. Effects of field propagation

For an optically thin medium, the dynamic equations (2.8-2.12) are enough to analyze the behavior of the system. Although, for an optically thick medium such as a long Rubidium vapor cell or a solid state medium, the propagation of the probe and drive fields should be taken into account. Under the slowly varying envelope approximation

[60], Maxwell's equations can be written as

$$\frac{\partial \Omega_1}{\partial z} + \frac{1}{c}\frac{\partial \Omega_1}{\partial t} = i\eta_1 \rho_{ab}; \tag{2.45}$$

$$\frac{\partial \Omega_2}{\partial z} + \frac{1}{c}\frac{\partial \Omega_2}{\partial t} = i\eta_2 \rho_{ac}; \tag{2.46}$$

where

$$\eta_i = \frac{3N\lambda_i^2 \gamma_i}{8\pi} \tag{2.47}$$

are the corresponding coupling constants (i=1,2), N is the density of atoms, and λ_i is the wavelength of the corresponding transition. These ordinary differential Eqs. (2.8-2.12), and the partial differential Eqs. (2.45-2.46) with proper initial ($t = 0$) and boundary conditions ($z = 0$) determine the evolution of the system.

Considering the probe and drive pulses $\Omega_1(t)$, $\Omega_2(t)$ are long enough, we can rewrite Eq. (2.10,2.12) as

$$\rho_{cb} = -\frac{\Omega_2 \Omega_1}{\Gamma_{ab}\Gamma_{cb} + |\Omega_2|^2}, \tag{2.48}$$

$$\rho_{ab} = -i\frac{\gamma_{cb}}{|\Omega_2|^2}\Omega_1 + \frac{1}{|\Omega_2|^2}\frac{\partial \Omega_1}{\partial t} \tag{2.49}$$

In the case that absorption is negligible and $\gamma_{cb} \simeq 0$, by plugging Eq. (2.49) into Eq. (2.45), we obtain

$$\frac{\partial \Omega_1}{\partial z} + \frac{1}{V_g(z,t)}\frac{\partial \Omega_1}{\partial t} = 0 \tag{2.50}$$

where $V_g = c/(1 + c\eta_1/|\Omega_2|^2) \simeq |\Omega_2|^2/\eta_1$. The solution of Eq. (2.50) is given by

$$\Omega_1(z,t) = \Omega_1\left(z - \int_{-\infty}^{t} V_g(z,t')dt'\right). \tag{2.51}$$

In the case γ_{cb} is small, the propagation equation is given by

$$\frac{\partial \Omega_1}{\partial z} + \frac{1}{V_g(z,t)}\frac{\partial \Omega_1}{\partial t} = -\frac{\gamma_{cb}\eta_1 \Omega_1}{\gamma_{ab}\gamma_{cb} + |\Omega_2|^2}. \tag{2.52}$$

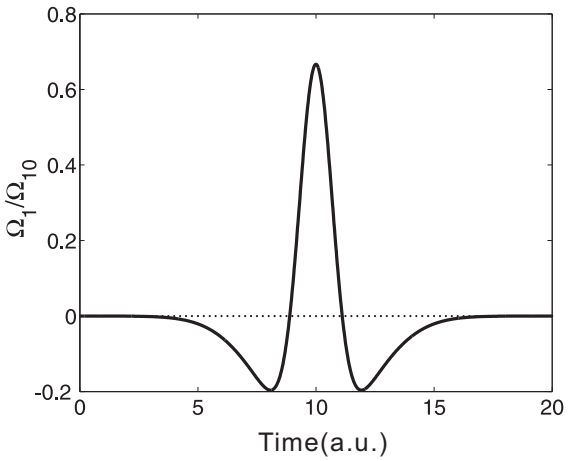

Fig. 4. Time dependence of pulse shape of $0-\pi$ -pulse with parameters $T_1 = 1$ and $T_2 = 3$

For small delay times, smaller than the duration of the drive pulse, such that

$$|\Omega_2|^2 \gg \frac{z}{V_g}\frac{\partial|\Omega_2|^2}{\partial t} \tag{2.53}$$

we can write the solution as

$$\Omega_1(z,t) = \Omega_1\left[z - \int_{-\infty}^{t} V_g(z,t')dt'\right]\exp\left[-\frac{\gamma_{cb}\eta_1 z}{\gamma_{ab}\gamma_{cb} + |\Omega_2|^2}\right] \tag{2.54}$$

where we can see the modification of the probe pulse shape due to the delay of the probe pulse by the group velocity and due to absorption.

C. Numerical simulations

It is known that the so-called $2n\pi$ pulses [59] can propagate through a medium of two-level atoms without absorption. In particular, we are interested in the propagation of weak optical pulses with the so called $0-\pi$ pulses that have larger propagation length in comparison with the Gaussian pulses that have small area.

In our simulations, we chose the Rabi frequency of the $0-\pi$ probe pulse to have

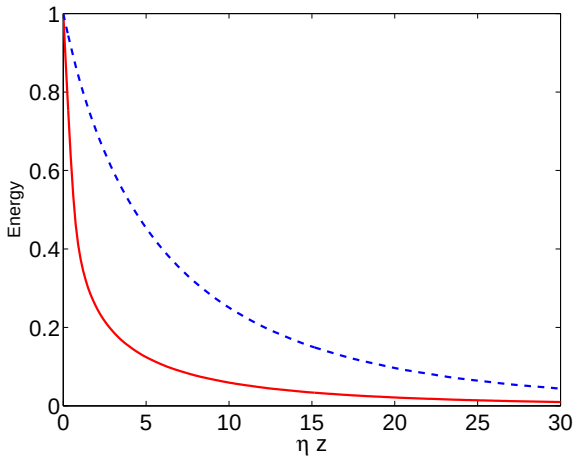

Fig. 5. Dependence of pulse energy on optical density. Gaussian pulse (red solid line) and $0-\pi$ pulse (blue dashed line)

the following time dependence

$$\Omega_1 = \Omega_{10}\left(e^{-\left(\frac{t-10}{T_1}\right)^2} - \frac{T_1}{T_2}e^{-\left(\frac{t-10}{T_2}\right)^2}\right), \tag{2.55}$$

where T_1 and T_2 are parameters. The shape of this probe pulse is shown in Fig. 4. It can be considered as the envelope of two Gaussian pulses. The first one has larger amplitude and shorter duration T_1, the second one has smaller amplitude and longer duration T_2. In our simulations, $T_1 = 1$, $T_2 = 3$, and the area of the pulse given by Eq.(2.55) is

$$\begin{aligned}\theta &= \int_{-\infty}^{\infty}\Omega(t')dt' \\ &= \Omega_{10}\int_{-\infty}^{\infty}\left(e^{-(t'-10)^2} - \frac{1}{3}e^{-\left(\frac{t'-10}{3}\right)^2}\right)dt' \\ &= \Omega_{10}(\sqrt{\pi}-\sqrt{\pi}) = 0\cdot\pi.\end{aligned} \tag{2.56}$$

In Figure 5, the propagation of the $0-\pi$ pulses is shown in comparison with the Gaussian pulse in the form

$$\Omega_2 = \Omega_{20}e^{-\left(\frac{t-10}{T_2}\right)^2} \tag{2.57}$$

where Ω_{10} and Ω_{20} are the initial amplitudes of the probe and drive pulses before

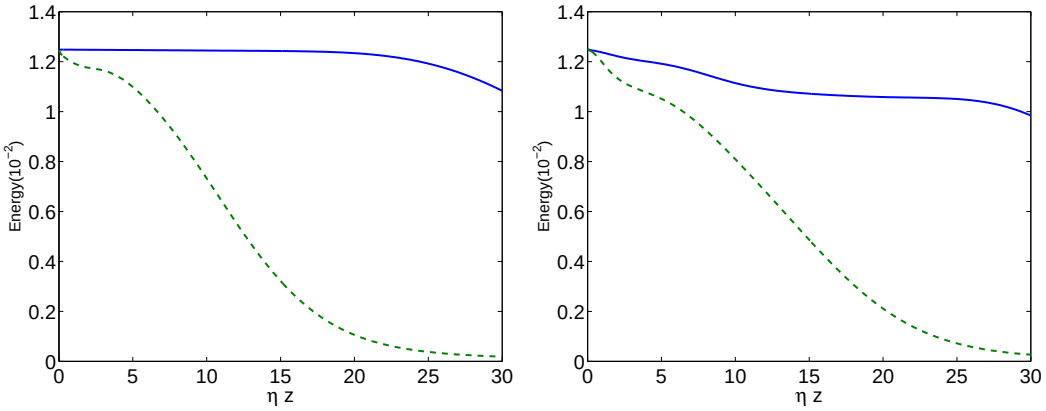

Fig. 6. Energy of Ω_1 versus position in the medium. Comparison for different driving fields Ω_2: Ω_2 is Gaussian pulse (solid line) and Ω_2 is $0-\pi$ pulse (dashed line). (Left) Ω_1 is Gaussian pulse. (Right) Ω_1 is $0-\pi$ pulse

the pulses enter the medium. Clearly, the absorption of the Gaussian pulses is larger than the $0-\pi$ pulse, and its propagation length is several times shorter.

To answer the interesting question of whether the propagation of pulses in EIT-configuration can be improved by using $0-\pi$-pulses instead of Gaussian pulses, we have performed simulation for a medium with optical density $3N\lambda^2 z/(8\pi)$, where z is the length of the medium, and N is the density of ^{87}Rb atomic gas.

Fig. 6 shows the dependence of the probe pulse energy on position, with $z = 10$, $\eta = 3$, $\rho_{bb} = 1$. Here we take Ω_1 to be the Gaussian pulse and $0-\pi$ pulse, and compare the difference when the driving fields are Gaussian pulse and $0-\pi$ pulse. The shape of the probe pulse is

$$\Omega_1 = \Omega_{p0} e^{-\left(\frac{t-10}{T_1}\right)^2} \tag{2.58}$$

for the Gaussian pulse. The driving pulse has amplitude $\Omega_{20} = 5$.

To compare the results, we consider these two types of drive pulses to have the same energy, and we introduce the coefficient 1.51 for the $0-\pi$ pulse initial amplitude.

In the top figure, Ω_1 is a Gaussian pulse, it shows that by switching the driving

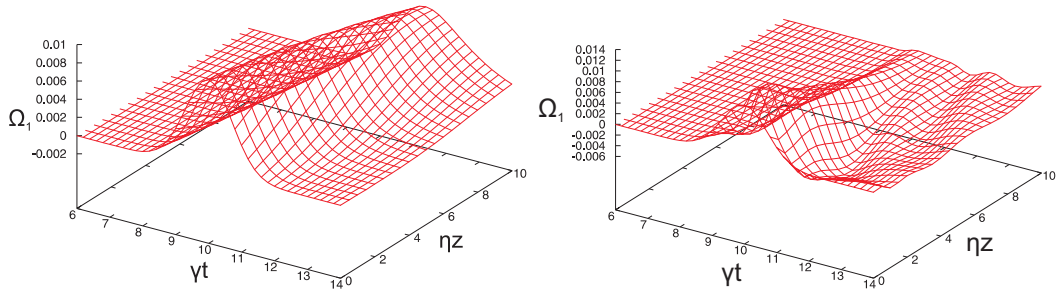

Fig. 7. Propagation of the Gaussian probe pulse, (Left panel) Ω_2 is Gaussian pulse and (Right panel) Ω_2 is $0-\pi$ pulse.

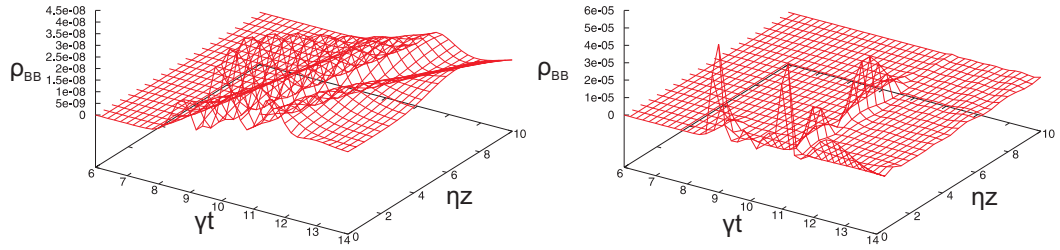

Fig. 8. Time-space dependence of population in the bright state. (Left panel) Ω_2 is Gaussian pulse and (Right panel) Ω_2 is $0-\pi$ pulse.

pulse between these two shapes, the probe pulse will have a large absorption for $0-\pi$ pulse or nearly no absorption for Gaussian pulse.

For the probe and drive pulses being both Gaussian we have perfect EIT. There is no absorption for the probe field. For the Gaussian probe and the $0-\pi$ drive pulses, we have practically no EIT, and the probe pulse is absorbed very fast. For the probe and drive pulses being both $0-\pi$ pulses, we also have no EIT, a result that is quite counter-intuitive. For the $0-\pi$ probe and the Gaussian drive pulses, we have some absorption but not as strong as we could expect-for the drive and probe pulses that have such different shapes, one would expect rather no EIT.

In Fig. 7, we plot propagation of the probe fields for Gaussian and $0-\pi$ drive fields. One can see that, for the case of Gaussian drive field, the probe field propagates without absorption. In the meanwhile for the $0-\pi$ drive field, the probe field absorbs

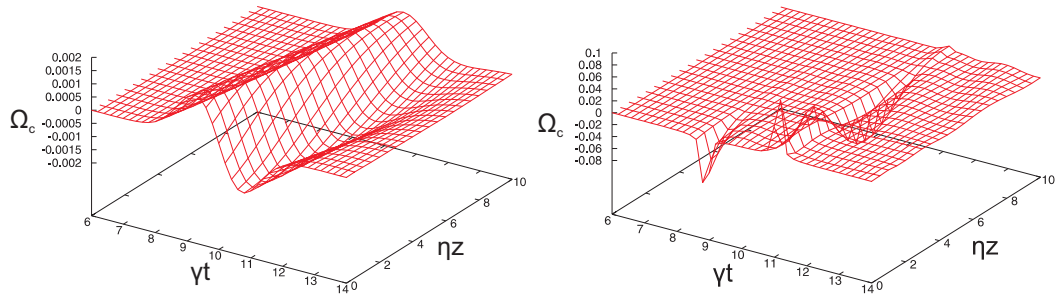

Fig. 9. Time-space dependence of coupling between the bright and dark states. (Left) Ω_2 is Gaussian pulse and (Right) Ω_2 is $0-\pi$ pulse.

very quickly. To gain physical insight, we plot population of the bright state for these cases in Fig. 8, and also we plot the coupling between the bright and the dark states in Fig. 9. It is clearly seen that, for the case of $0-\pi$ drive field, the population of the bright state is much larger (See Fig. 8) and the coupling between the bright and the dark states is also much stronger.

Surprisingly, for the case of $0-\pi$ probe pulse, we observe similar behaviors as shown in Fig. 10. We have a better propagation for the Gaussian drive than for the $0-\pi$ drive pulse. Intuitively, one would expect that the absorption for the matching pulses, the $0-\pi$ pulses in this case, should be smaller than the case when driving pulse is Gaussian.

The physical reason for such a counter-intuitive behavior is the strong dispersion of the resonant medium that the probe pulse experiences during propagation. It is interesting to see the evolution of the pulses that has a spectral hole. Such pulse can propagate through the medium according to Eq. (2.51), and as it is shown in Fig. 11. It causes the delay of the probe pulse and some reshaping of the pulse. Even initially before entering the medium, the probe drive pulses have been matched. Due to the strong dispersion, the probe delays from the drive pulse and it gives rise to the coupling between the dark and the bright states. The level of this coupling is

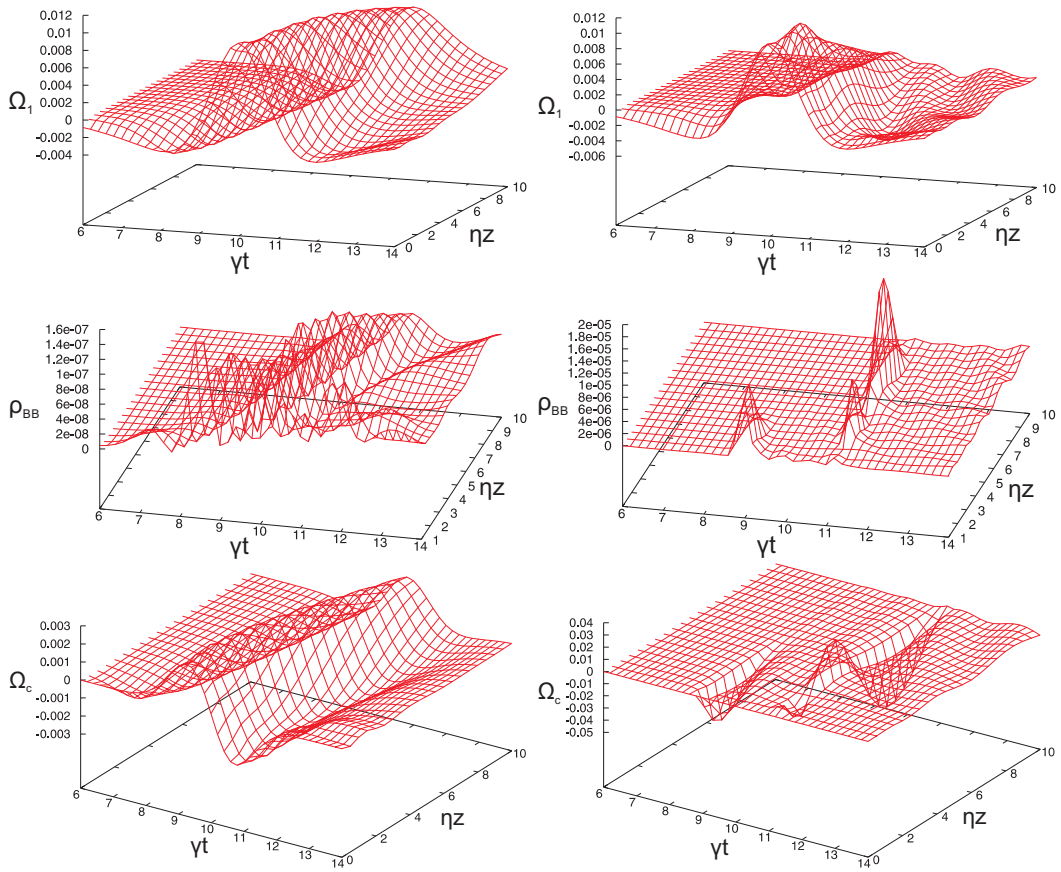

Fig. 10. Propagation of the $0-\pi$-probe pulse, (Left panel) Ω_2 is Gaussian pulse and (Right panel) Ω_2 is $0-\pi$ pulse.

different for different shape of the pulses. It turns out that the Gaussian pulses are more tolerant of reshaping and delays. That explains why the Gaussian drive pulses give us better propagation results.

D. Application of obtained results

1. Control of propagation

As it has been shown above, when the drive pulse is $0-\pi$ pulse, the probe pulse has larger absorption; and when the probe pulse is a Gaussian pulse, the probe pulse passes through the medium practically without absorption. It allows for an all-optical

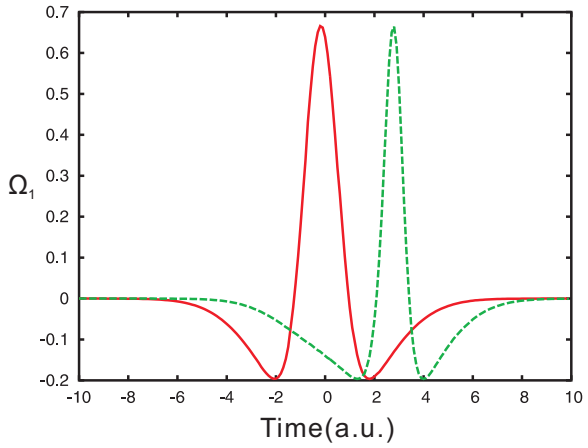

Fig. 11. The probe pulse snapshots at different locations during propagation in a three--level Λ medium. Area of the pulse is initially zero (red solid curve), after some distance, the pulse (green dashed curve) is delayed, and its area is not zero.

switch. It can be achieved by controlling the shape of the drive pulse in Fig. 6.

The scheme is shown in Fig. 12. A Gaussian drive pulse with frequency resonant with the transition $|a\rangle - |b\rangle$ is generated by a laser system. Then, the pulse interacts with a partially transparent mirror M1 that allows for a small amount of the pulse energy to pass through and to reflect the most of the pulse energy. The part that passes through the mirror is used as the probe pulse, and the reflected part is used as the drive pulse. The probe pulse is fully reflected by mirrors M2 and M4. The drive pulse passes through an optical parametric amplifier (OPA) and a pulse shaper. The OPA changes the frequency of the drive pulse to be resonant with the transition between $|a\rangle - |c\rangle$. The pulse shaper controls the pulse shape. Two paths for the probe and drive pulses are adjusted to have the same distance, so that they can reach the semitransparent mirror M3 simultaneously, which enables the drive pulse to fully pass through and enables the probe pulse to be fully reflected.

If we change the drive pulse shape to $0-\pi$ pulse, then the probe pulse has a large absorption and cannot pass through the Λ medium. In this case, the detector can

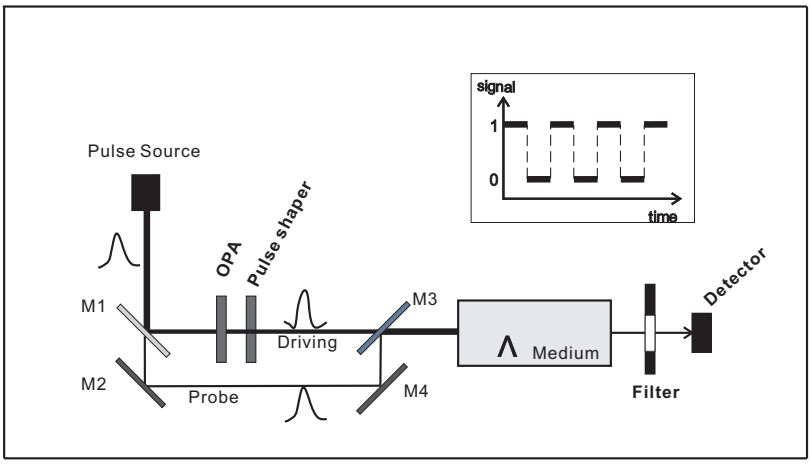

Fig. 12. All-optical switch.

detect nothing. This is equivalent to the output of signal 0. If the drive pulse shape is the Gaussian, then the probe pulse propagates through this medium. In this case, the detector can detect the probe pulse, which is equivalent to the output signal of 1. Using the controlled pulse shaper, we are able to control whether the probe pulse passes through the medium or not and generate any sequences of the probe pulses. This can have application in all-optical computing. This is a new way to control the propagation, namely, by using different shapes of drive pulses, we can control transparency of the medium for the probe pulses. The most interesting part is to have nearly 100% absorption. In this situation, the change of the drive pulse allows us to implement an all-optical switching. The advantage of our proposal is that we do not need a mechanical part to physically switch on or off the drive pulse as has been done in [61], where they have successfully made the EIT based optical switch by turning on or off of the drive field periodically. Instead, we continuously change the drive pulse shape by using the pulse shaper that introduces phases to different spectral components of the drive pulse.

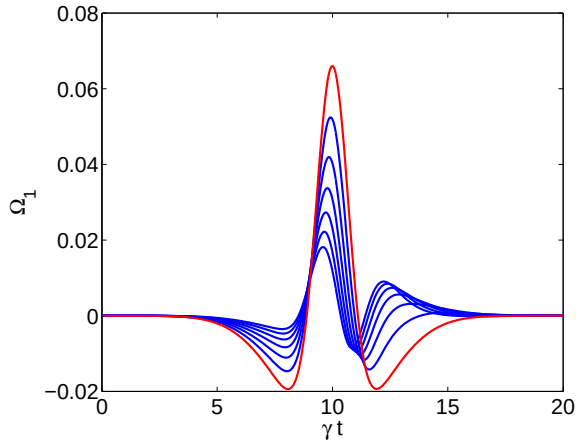

Fig. 13. Dependence of pulse shape on time at different positions inside medium.

2. Hole filling effect

The $0-\pi$ probe pulse shapes on different spatial positions with detuning $\Delta = 0$ are shown in Fig. 13. Here we use the following parameters: $\Omega_{10} = 0.1, \Omega_{20} = 5$, $\rho_{bb} = 1$, $\gamma = 0.1$. Due to the stimulated Raman process, the high intensity part of the probe pulse is more influenced by the nonlinear interaction than a relatively weak part. This leads to a modification of the intense part of the pulse with respect to a weaker part, and influences on the pulse shape. As we have mentioned, the input $0-\pi$ pulse has an initial area to be equal to zero, any change of area is easy to observe because the area is related to the same frequency of the probe pulse that has zeroth amplitude. Change of the pulse area means that this "zeroth" amplitude changes and this process can be referred to as a "hole filling effect." It is interesting to study the change of the pulse area with the change of pulse shape. This influence can be shown more clearly in the dependence of the pulse shape on time at different positions inside the medium, as shown in Fig. 13

To make it clearer, in Figure 14, we show the spectrum of the probe pulse at three different positions: at the initial input, at the middle of the medium and at the

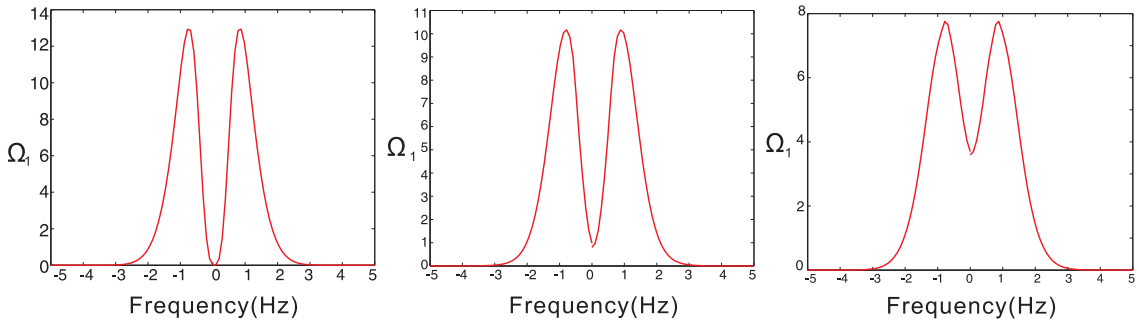

Fig. 14. Spectrum of Probe pulse Ω_1. (L) Input pulse spectrum. (M) Pulse Spectrum in the middle of medium (R) Output pulse spectrum

output. It can be seen that initially there is a spectral hole in the middle of pulse spectrum, which is related to the fact that the input is the $0 - \pi$ pulse and it has the zero area. While the pulse is propagating through the medium, the spectral hole is partially filled; the longer distance it passes, the more the hole is filled, which can be seen from the second and third figures. Through the level of hole filling, one can obtain the density of the atoms or molecules in the medium.

It is interesting to see the evolution of the pulses that has a spectral hole. Such pulse can propagate through the medium according to Eq. (2.51), and as it is shown in Fig. 11. One can see that due to time delay, the area of the pulse changes, as shown in Fig. 14. We can also see the change of the spectrum of the probe pulse during its propagation.

These results suggest a new approach to Raman spectroscopy that extends application of the stimulated Raman scattering to media that have a lot of scattering. The stimulated Raman scattering has an advantage of relaxing phase-matching condition which is difficult or even impossible to meet under condition of strong scattering. This technique is compatible and can be applied to microscopy.

E. Conclusion

In conclusion, we presented a theoretical study of Electromagnetically Induced Transparency (EIT) with $0-\pi$ pulses. We simulated the propagation of $0-\pi$ laser pulses through a medium of three-level $\Lambda-type$ atoms, and compared with Gaussian co-propagating pulses. We found that even on two-photon resonance the absorption of the $0-\pi$ pulses is significantly greater than that of the Gaussian pulses. We used the dark and bright basis to explain the behavior, and discussed possible applications.

We studied the effects of pulse shape on the efficiency of Electromagnetically Induced Transparency (EIT). As a single $0-\pi$ pulse experiences less absorption than a Gaussian pulse of the same energy, we researched whether using $0-\pi$ pulses instead of Gaussians as probe pulses in EIT will result in less absorption. It turned out that this is not the case, but quite the opposite. When using $0-\pi$ pulses as the probes in EIT, the absorption is increased. The explanation of this counter-intuitive result is elegantly illustrated in the dressed state basis. The time dependance of the $0-\pi$ pulse results in an interaction between the dark and the bright state which decouples the dark state population and hence increases absorption. The effect may find a possible application in developing an all-optical switch.

Future work includes studying the effects of propagation of $0-\pi$ pulses in the spectral domain [62], as such pulses have applications on nonlinear spectroscopy in scattering media [63].

CHAPTER III

NONLINEAR SPECTROSCOPY WITH $0 - \pi$ PULSES

A. Introduction

Raman spectroscopy [64] is a powerful tool widely used in engineering, chemical, and biological applications [64, 65]. However, multiple scattering decreases sensitivity and limits its applications to live tissues and to media consisting of bacterial spores because of high level of noise coming from scattered light. Recently, sensitivity of coherent Raman scattering has been improved by applying femtosecond adaptive technique to excite maximal vibrational coherence in media consisting of test molecules to perform real time identification of bacterial spores [66, 67], and this technique has a lot of potential to identify biomoleculars as well.

The idea of current approach is to apply the pulse shaping technique to stimulated Raman scattering to enhance its sensitivity and to extend the application of the technique to the situations where there is strong light scattering in the media. Let us note that the method we use here is similar to the one suggested in [68] for detection of two-photon absorption.

To illustrate how the idea works, let us consider a gas of molecules interacting with two laser pulses (energy levels and configuration of laser fields are shown in Fig. 15). The frequency difference of laser pulses is close to the two-photon resonance with the molecular vibrational transition. The first laser pulse, corresponding Rabi frequency given by $\Omega_1(t) = \Omega_{10} \exp[-(t/T)^2]$, is chosen to be gaussian (see Fig.16(a)), and the second laser pulse is a specially generated pulse form that has a waveform, for example, as

$$\Omega_2(t) = \Omega_{20}[\exp\left(-\frac{t^2}{T^2}\right) - \frac{T}{T_2}\exp\left(-\frac{t^2}{T_2^2}\right)], \tag{3.1}$$

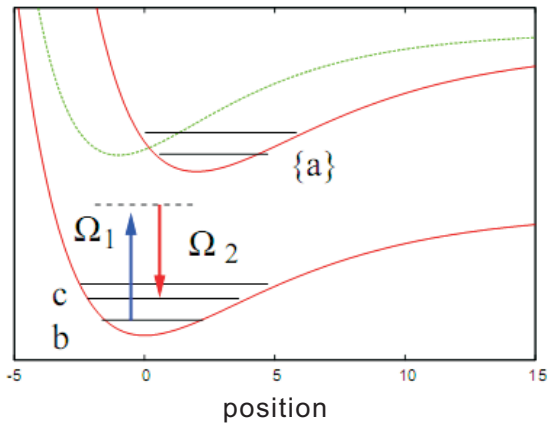

Fig. 15. Raman transition in a molecular medium, probed by a pump pulse Ω_1 and a Stokes pulse Ω_2.

where T and T_2 are parameters of the envelop (see Fig.16(b)), of which the area is equal to zero, so these pulses are referred to as so-called $0-\pi$ pulses. The pulse spectrum is given by

$$\begin{aligned} S_2(\omega) &= \Omega_{20} \int dt e^{-i\omega t} \Omega_2(t) \\ &= \Omega_{20} T[\exp\left(-\frac{T^2\omega^2}{2}\right) - \exp\left(-\frac{T_2^2\omega^2}{2}\right)]. \end{aligned} \tag{3.2}$$

The spectrum of probe pulse is shown in Fig.17(a). An important feature of the pulse is that its spectrum has a spectral hole at the center frequency. Stimulated Raman process is nonlinear, thus high intensity part of the pulse is more influenced by nonlinear interaction than a relatively weak part. This leads to different modification of the intense part of the pulse with respect to the weaker part, and influence on the pulse spectrum. Thus, as a result, after propagation through the medium, the spectral hole of the pulse is filled due to nonlinear stimulated Raman process (see 17(b)). Detecting the hole filling allows one to obtain spectroscopic information about specific molecules.

This chapter is organized as follows. The model and simple estimation are pre-

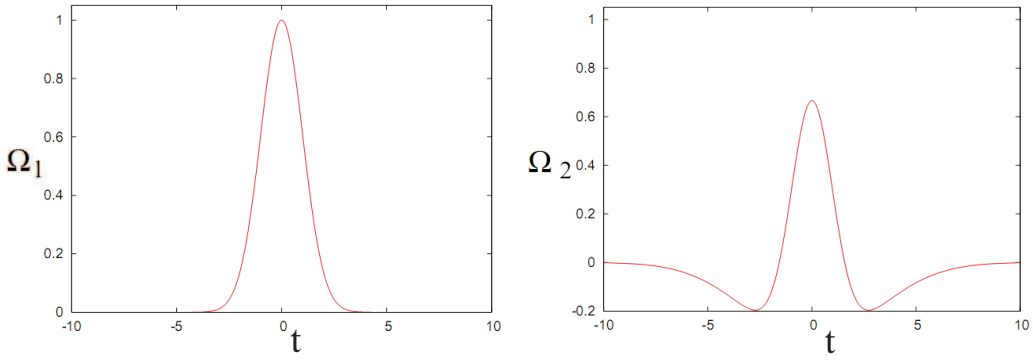

Fig. 16. The pump pulse Ω_1 has a Gaussian profile (a), while the Stokes pulse Ω_2 is a $0-\pi$ pulse(area is 0)(b).

sented in Section II. From simple pulse waveforms for which the calculation can be done analytically, we show that the approach works.

B. Model and estimations

The vibrational energy level of molecule is shown in Fig.15. We apply two laser pulses, driving pulse $\mathcal{E}_1$ and probe pulse $\mathcal{E}_2$. The interaction Hamiltonian for the system is given by

$$V_I = -\hbar[\Omega_2 e^{-i\omega_{ac}t}|a\rangle\langle c| + \Omega_1 e^{-i\omega_{ab}t}|a\rangle\langle b| + h.c.] \tag{3.3}$$

$\Omega_i = \wp_i \mathcal{E}_i/\hbar$ is the Rabi frequency of the respective fields; $\wp_{ab}$ and $\wp_{ac}$ are the electrical dipole matrix elements between states a and b, and a and c; ω_{ab} and ω_{ac} are the frequencies of the electronic transitions; ω_{cd} and ω_{db} are the frequencies of the vibrational and rotational transitions; $\mathcal{E}_i$ is the amplitude of the respective laser field.

The time-dependent density matrix equations are

$$\frac{\partial \rho}{\partial \tau} = -\frac{i}{\hbar}[H, \rho] - \frac{1}{2}(\Gamma\rho + \rho\Gamma), \tag{3.4}$$

where Γ is the relaxation matrix. A self-consistent system also includes the field

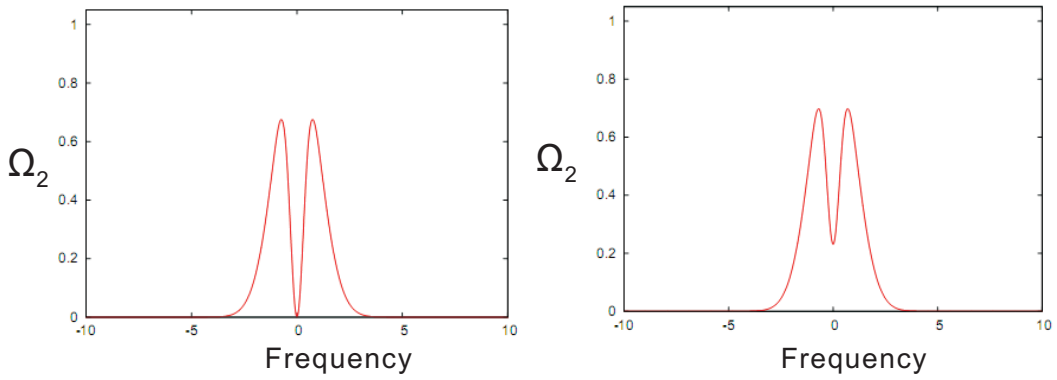

Fig. 17. The spectral profile of probe pulse Ω_2. (a) Before interacting with medium, there is a hole at the central frequency (b) After interacting with medium, the spectral hole in the Stokes profile is partially filled

propagation equations

$$\frac{\partial \Omega_\alpha}{\partial z} = -\kappa_\alpha \Omega_\alpha + i\eta_\alpha \rho_\alpha, \tag{3.5}$$

where, index $\alpha = 1, 2$ indicates corresponding field and polarization between levels $|a\rangle \leftrightarrow |b\rangle, |a\rangle \leftrightarrow |c\rangle$; $\eta_\alpha = \nu_\alpha N \wp_\alpha^2/(2\hbar\epsilon_0 c)$ is the corresponding coupling constant; $\nu_{1,2}$ is the frequency of the optical field, N is the density of medium, ϵ_0 is the permitivity of the vacuum, c is the speed of light in vacuum, and κ_i are losses of the field during propagation in the cell because of scattering, diffraction, or non-resonant absorption.

Before turning to simulations, to gain physical insight, it is instructive to perform estimations in the simple approximation that all populaiton is in level b. The equations for optical polarization and vibrational coherence are the following

$$\dot{\rho}_{ab} = -\Gamma_{ab}\rho_{ab} - i\Omega_1 - i\rho_{cb}\Omega_2 \tag{3.6}$$

$$\dot{\rho}_{ca} = -\Gamma_{ca}\rho_{ca} + i\rho_{cb}\Omega_1, \tag{3.7}$$

$$\dot{\rho}_{cb} = -\Gamma_{cb}\rho_{cb} - i\Omega_2\rho_{ab} + i\Omega_1\rho_{ca}, \tag{3.8}$$

where $\Gamma_{ab} = \gamma_{ab} + i(\omega_{ab} - \nu_1)$, $\Gamma_{ca} = \gamma_{ac} - i(\omega_{ac} - \nu_2)$ $\Gamma_{cb} = \gamma_{cb} + i(\omega_{cb} - \nu_1 + \nu_2)$ same as they are defined in Eq.(2.13-2.15).

First, let us consider laser fields being in resonance with corresponding optical transitions, $\omega_{ab} = \nu_1$ and $\omega_{ac} = \nu_2$, and the laser pulses with their durations that are longer than the relaxation time of optical polarization, but shorter than the relaxation time of the vibrational coherence. Then the optical polarizations are given by

$$\rho_{ab} = -\frac{i\Omega_1 + i\rho_{cb}\Omega_2}{\Gamma_{ca}}, \quad \rho_{ca} = \frac{i\rho_{cb}\Omega_1}{\Gamma_{ca}}, \tag{3.9}$$

and the equation for ρ_{cb} becomes

$$\dot{\rho}_{cb} = -(\Gamma_{cb} + \frac{|\Omega_2|^2}{\Gamma_{ab}} + \frac{|\Omega_1|^2}{\Gamma_{ca}})\rho_{cb} - \frac{\Omega_1\Omega_2}{\Gamma_{ab}} \tag{3.10}$$

Two cases should be distinguished. The first case is when the optical pulses are weak

$$(\frac{|\Omega_2|^2}{\Gamma_{ab}} + \frac{|\Omega_1|^2}{\Gamma_{ca}})\tau \ll 1 \tag{3.11}$$

where τ is the duration of the laser pulses, and

$$\rho_{cb} = -\int_{-\infty}^{t} dt' \frac{\Omega_1\Omega_2}{\Gamma_{ab}}. \tag{3.12}$$

Note here that if we would have large detuning, then formally the off-resonant case would be fitting this one.

The second case is when the pulses are strong and the power broadening terms are leading in Eq.(3.10),

$$(\frac{|\Omega_2|^2}{\Gamma_{ab}} + \frac{|\Omega_1|^2}{\Gamma_{ca}})\tau \gg 1 \tag{3.13}$$

and then

$$\rho_{cb} = -\frac{\Omega_1\Omega_2}{\Gamma_{ab}(\Gamma_{cb} + \frac{|\Omega_2|^2}{\Gamma_{ab}} + \frac{|\Omega_1|^2}{\Gamma_{ca}})} \simeq -\frac{\Omega_1\Omega_2}{|\Omega_2|^2 + |\Omega_1|^2}. \tag{3.14}$$

The propagation of field Ω_2 is governed by

$$\frac{\partial \Omega_2}{\partial z} = -\kappa_2 \Omega_2 + i\eta \rho_{ca}, \tag{3.15}$$

where κ_2 is the depletion of the field Ω_2 during propagation due to background absorption or scattering. Using Eq.(3.9), we obtain

$$\frac{\partial \Omega_2}{\partial z} = -\kappa_2 \Omega_2 + \eta \frac{\rho_{cb}\Omega_1}{\Gamma_{ca}}, \tag{3.16}$$

For regime of strong fields $|\Omega_1| \gg |\Omega_2|$, using Eq.(3.14), we can see that Eq.(3.16) gives us gain $\eta/\Gamma_{ca} - \kappa_2$ via stimulated Raman amplification [69]. For weak field regime (Eq.(3.11), the propagation of the pulse Ω_2 is more complicated. In both cases, the shape of pulse Ω_2 after propagation depends on the shape of pulse Ω_1 because of the nonlinear term in Eq.(3.16).

Indeed, a spectral component of field Ω_2 is defined as

$$\Omega_{2\omega}(z) = \int \Omega_2(t,z) e^{i\omega t} dt, \tag{3.17}$$

and now we can write

$$\int \frac{\partial \Omega_2(t,z)}{\partial z} e^{i\omega t} dt = -\int (\kappa_2 \Omega_2 - \eta \frac{\rho_{cb}\Omega_1}{\Gamma_{ca}}) e^{i\omega t} dt \tag{3.18}$$

that brings us to the propagation equation for spectral components of $\Omega_{2\omega}(z)$ as

$$\frac{\partial \Omega_{2\omega}}{\partial z} = -\kappa_2 \Omega_{2\omega} + \frac{\eta}{\Gamma_{ca}} \int \rho_{cb}\Omega_1 e^{i\omega t} dt. \tag{3.19}$$

From Eq.(3.19), we see that every spectral component of field $\Omega_{2\omega}$ experiences depletion due to κ_2, and also contribution from all other spectral components contributed by the nonlinear term. Thus, if initially we have a spectral hole, $\Omega_{2\omega=0}(z=0) = 0$, it is going to be filled while the pulse propagates through the medium.

Let us define a signal as a normalized zero-frequency frequency component of

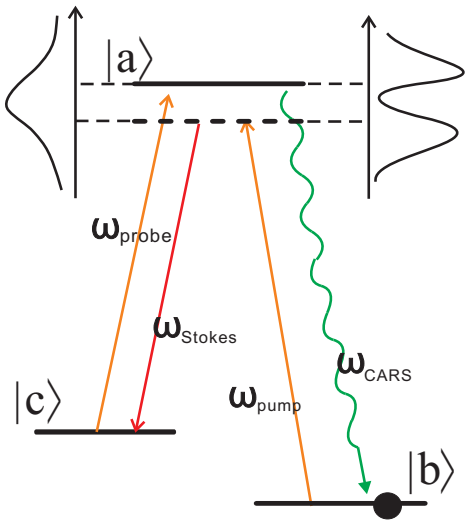

Fig. 18. Spectral picture of hole filling. Spectral components of both pulses create coherence and then the new frequency component of Ω_2 is generated to fill in the hole in the spectrum.

Stokes field after propagation distance L, which is given by

$$S_2 \equiv \frac{\Omega_{2\omega=0}(z=L)}{\Omega_{20}} \tag{3.20}$$

then for weak pulses we assume that

$$\frac{\partial S_2}{\partial z} = \frac{\eta}{\Gamma_{ca}} \int dt \Omega_1(t) e^{i\omega t} \int_{-\infty}^{t} dt' \frac{\Omega_1(t')\Omega_2(t')}{\Gamma_{ab}} \tag{3.21}$$

$$\Omega_{2\omega} = \alpha_\omega \exp[-\kappa_2 z] \tag{3.22}$$

where

$$\alpha_w = \int dt \alpha(t) e^{i\omega t} \tag{3.23}$$

$$S_2 = \frac{\eta z}{\Gamma_{ab}\Gamma_{ca}} \int dt \Omega_1(t) e^{i\omega t} \int_{-\infty}^{t} dt' \Omega_1(t')\alpha(t') \tag{3.24}$$

Signal does not depend on the linear absorption coefficient κ_2.

The physics of the generated signal can be seen in Fig. 18. Even though the configuration of the fields corresponds to stimulated Raman scattering, the process

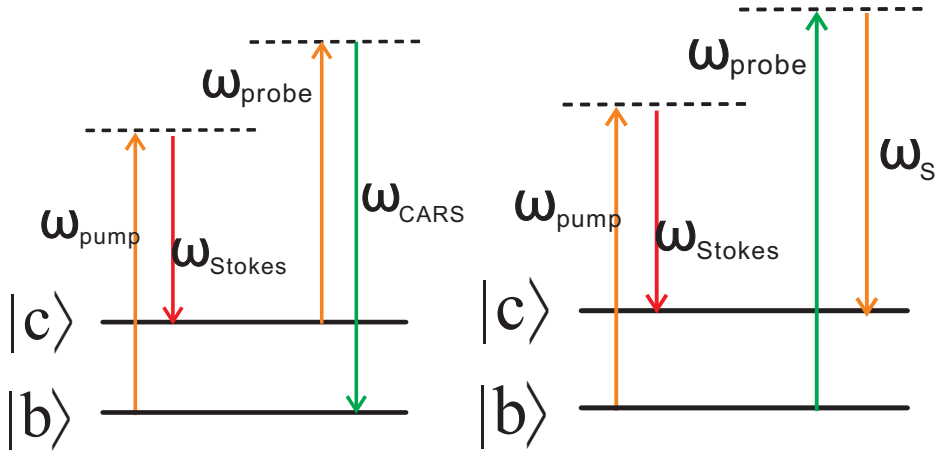

Fig. 19. Configuration of pulses for CARS(left) and CSRS(right). $|b\rangle$ and $|c\rangle$ are vibrational states of molecules. In CARS, the probe pulse is applied between ground state $|c\rangle$ and virtual states; while in CSRS, the probe pulse is applied from the ground state $|b\rangle$ to the virtual state.

behind the hole filling is three-wave mixing. Indeed, in Fig. 19(a) we show configuration of fields for CARS where two fields generate coherence between levels $|b\rangle$ and $|c\rangle$, and then coherent scattering of the signal field leads to the generation of anti-Stokes coherent beam with frequency $\omega_{CARS} = \omega_{pump} - \omega_{Stokes} + \omega_{probe}$. The generation of coherent Stokes beam is similar to CARS (see Fig. 19b). One can see that the hole filling is similar to CSRS. Spectral components of pump and Stokes pulses create vibrational coherence between levels $|b\rangle$ and $|c\rangle$, and then spectral component 3 has component 4 which scatters into the spectral hole of 0π-pulse Ω_2.

Equation (3.24) can be rewritten as

$$S_2 = \frac{\eta z}{\Gamma_{ab}\Gamma_{ca}} \int_{-\infty}^{\infty} dt \int d\omega_1 d\omega_2 d\omega_3 \frac{\exp[i(\omega_1 - \omega_2 + \omega - \omega_3)t]}{i(\omega_1 - \omega_2)} \Omega_{1\omega_3} \Omega^*_{1\omega_1} \alpha_{\omega_2} \qquad (3.25)$$

Because the frequencies of laser beams are very close, the phase-matching condition is always fulfilled.

It is instructive to see the effect for some analytical waveforms. Let us consider

a few examples. First, we consider the gaussian pulses given by

$$\Omega_1(t) = \Omega_{10}[\exp(-\frac{t^2}{T^2}) \tag{3.26}$$

$$\Omega_2(t) = \Omega_{20}[\exp(-\frac{t^2}{T^2}) - \frac{T}{T_2}\exp(-\frac{t^2}{T_2^2})], \tag{3.27}$$

then the signal is given by

$$\begin{aligned} S_2 &= \frac{\eta z}{\Gamma_{ab}\Gamma_{ca}} \int dt \Omega_1(t) e^{i\omega t} \int_{-\infty}^{t} dt' \Omega_1(t') \alpha(t') \\ &= \frac{\pi}{4}\left(\sqrt{2} - 2\sqrt{\frac{T^2}{T^2+T_2^2}}\right) \frac{\eta L T^2 |\Omega_{10}|^2 |\Omega_{20}|}{\Gamma_{ab}\Gamma_{ca}}. \end{aligned} \tag{3.28}$$

.

Second, let us consider the pulses that are given by

$$\Omega_1(t) = \Omega_{10}\exp(-(\frac{t}{T})^2) \tag{3.29}$$

$$\Omega_2(t) = 2\Omega_{20} t \exp(-(\frac{t}{T})^2) \tag{3.30}$$

the signal in this case is

$$S_2 = \sqrt{\frac{\pi}{12}} \frac{\eta L T^2 |\Omega_{10}|^2 |\Omega_{20}|}{\Gamma_{ab}\Gamma_{ca}} \tag{3.31}$$

The third example of pulses is

$$\Omega_1(t) = \Omega_{10}\cos(\frac{t}{T})\theta(\frac{\pi}{2} - |\frac{t}{T}|) \tag{3.32}$$

$$\Omega_2(t) = \Omega_{20}\cos(\frac{t}{T_2})\cos(\frac{3t}{T_2})\theta(\frac{\pi}{2} - |\frac{t}{T}|), \tag{3.33}$$

and the signal is

$$S_2 = \frac{4}{15} \frac{\eta L T^2 |\Omega_{10}|^2 |\Omega_{20}|}{\Gamma_{ab}\Gamma_{ca}} \tag{3.34}$$

Summarizing the results above, we can write

$$\frac{S_2}{\Omega_{20} T} = \frac{\eta L T |\Omega_{10}|^2}{\Gamma_{ab}\Gamma_{ca}} \xi \simeq \frac{\eta L T |\Omega_{10}|^2}{\Gamma_{ab}\Gamma_{ca}} \tag{3.35}$$

Table I. The minimal atomic and molecular density estimated by Eq.(3.37).

Atom/Molecule	Rb	Cs	I_2	Br_2	CO	NO	R6G
Pulse duration, T	10 ns	10 ns	30 ps	30 ps	3 ps	3 ps	100 fs
λ	780 nm	852 nm	560 nm	560 nm	300 nm	300 nm	590 nm
γ_r [in s^{-1}]	$3.81 \cdot 10^7$	$3.33 \cdot 10^7$	10^8	10^8	10^8	10^8	10^8
Density [in cm^{-3}]	10^7	10^7	10^{10}	10^{10}	10^{13}	10^{13}	10^{15}

where $\Omega_{\alpha 0}$ is the maximum amplitude of corresponding field Ω_α, and ξ is defined as

$$\xi = \int_{-\infty}^{\infty} dt/T \frac{\Omega_1(t)}{\Omega_{10}} \int_{-\infty}^{t} \frac{\Omega_1(t')\Omega_2(t')}{\Omega_{10}\Omega_{20}} dt'/T \tag{3.36}$$

which is of the order of 1, $0 < \xi \leq 1$, and depends on the shape of the pulses.

We can estimate the density sensitivity by

$$N \simeq \frac{8\pi\Gamma_{ab}\Gamma_{ca}}{3\lambda^2 L\gamma_r T\Omega_{10}^2} \tag{3.37}$$

The results are shown in Table I, where we use the parameters of atoms (Rb, Cs), simple molecules with either electronic optical transitions (I_2, Br_2), or IR transitions between vibrational states (CO, NO), dye molecules, such as R6G, DMS, piridin, in solution [67].

For stronger pulses, we have

$$\frac{\partial S_2}{\partial z} = \frac{\eta}{\Gamma_{ca}} \int dt e^{i\omega t} \frac{\Omega_1^2 \alpha}{\Gamma_{cb}\Gamma_{ab} + |\alpha|^2 \exp[-2\kappa_2 z] + |\Omega_1|^2} \tag{3.38}$$

and for drive field much stronger than probe field $\Omega_1 \gg \Omega_2$, we have

$$\frac{\partial S_2}{\partial z} = \frac{\eta}{\Gamma_{ca}} \int dt e^{i\omega t} \frac{\Omega_1^2 \alpha}{\Gamma_{cb}\Gamma_{ab} + |\Omega_1|^2} \tag{3.39}$$

and the signal no longer depends on the κ_2. Also, let us note here that for too strong field $|\Omega_1|^2$, the signal is saturated by a factor $G = 1 + |\Omega_1|^2/\Gamma_{ab}\Gamma_{cb}$.

C. Conclusion

In conclusion, we suggest an approach that extends the application of the stimulated Raman scattering to media which have a lot of scattering. The stimulated Raman scattering has an advantage of relaxing phase-matching condition which is difficult or even impossible to meet under condition of strong scattering. This technique can be applied to microscopy.

CHAPTER IV

COLLISION INDUCED COHERENCE IN PLASMA AND BRANCHING RATIO IN MULTILEVEL SYSTEM

A. Introduction

An excited free atom decays into a vacuum emitting spatially isotropic radiation in the spectrum of frequencies which has Lorentzian shape with a bandwidth proportional to the Einstein A coefficient [70]. The decay rate is a combination of fundamental atomic constants and strongly resistant to a modification. However, such modifications are possible, for instance when the atom is no longer free and placed in a high-Q wavelength-size cavity. The decay of the strongly confined atom has been the subject of intensive theoretical and experimental research[71]. Here, the rate is enhanced or suppressed through the modification of the density of electromagnetic modes in the neighborhood of the resonant frequency[72]-[74]. Using a three-level atom driven by coherent fields is another way to control the spontaneous emission [75] and observe narrowing of spectral linewidth compared to the natural linewidth [76, 77]. Four-level driven atomic configurations offer yet another level of control allowing, for example, spectral line elimination and full spontaneous emission cancelation [78, 79].

The topic of above-mentioned studies has been focused on individual transitions in atoms and addressed the modification of one or another rate of spontaneous radiative decay. A number of studies consider more involved schemes characterized by correlated emission simultaneously from two atomic upper levels. Such type of interference of decay channels has been exploited, for instance, by Harris in his proposal of lasing without inversion in [80]. In contrast to most studies, we consider not the direct interference of decay channels, but rather the interference of incoherent

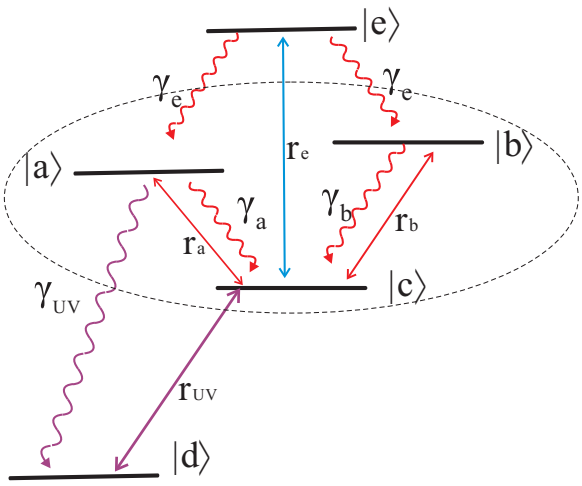

Fig. 20. Five-level configuration of working levels. The three-level subsystem $|a\rangle - |c\rangle - |b\rangle$ (inside the oval) is the core for the study of the suppression of the spontaneous emission on the visible transition. Here γ_a and γ_b are spontaneous decay rates and r_a and r_b are collision-assisted pumping rates. For simplicity they are set pairwise equal: $\gamma_a = \gamma_b \equiv \gamma_{vis}$, $r_a = r_b \equiv r_{vis}$. The $|a\rangle \leftrightarrow |d\rangle$ is the ultraviolet transition along which the spontaneous emission proceeds in a regular fashion with rate γ_{UV}. The pumping rate r_e to state $|e\rangle$ with simultaneous equal decay rates γ_e to states $|a\rangle$ and $|b\rangle$ is important as these processes pump the collision-induced dark state, as explained in the text. The rate r_d serves to close the system. Note that pumping rates along all dipole-allowed transitions are present in plasmas. The particular value of the rate depends on the energy of the transition according to the Boltzman distribution.

pumping rates (namely, collision-induced interference). In its turn, this interference induces the correlation in spontaneous emission. We propose using branching ratio R as the measure of this correlation. The term branching ratio here stands for the ratio of two spontaneous decay rates from two upper levels $|a\rangle$ and $|b\rangle$ to two lower levels $|c\rangle$ and $|d\rangle$ in a five-level atom of Fig.20:

$$R = \frac{\gamma_{vis}}{\gamma_{UV}} \tag{4.1}$$

where for definition we formulate the branching ratio in terms of decay rates on visible, γ_{vis}, and ultraviolet,γ_{UV}, transitions. Here, we refer to particular transitions in order to keep a close link to the previous experiments on measurements of changes of branching ratios. These experiments were performed in plasmas in Princeton by Suckewer and coworkers [81]. They serve as the main motivation and reference point of our study, although our results are applicable to more general schemes.

The branching ratio is closely related to total spectral-line intensities (in photons) for the two transitions, I_{vis} and I_{UV}. This relation is simply the consequence of the fact that the intensities are proportional to corresponding decay rates (for schemes considered so far): $I_{vis} \propto \gamma_{vis}$ and $I_{UV} \propto \gamma_{UV}$. In fact, this proportionality allows us to consider the intensity as alternative operational definition of the decay rate which differs from the pure decay rate by a factor. The access to this factor can be, however, a difficult experimental task. This potential experimental problem disappears when we consider the branching ratio. In those cases where the radiation is emitted from same level(s) the factors are the same for both transitions and therefore cancels out in the ratio in Eq. (4.1). So, the operational definition of the branching ratio can be introduced as

$$R = \frac{I_{vis}}{I_{UV}} \tag{4.2}$$

Moreover, for some cases, including ours, the operational definition in Eq. (4.2) is very natural and probably the only possible definition. The problem is that we consider simultaneous decay along two (visible) transitions. This decay is characterized by more than one decay rate. This problem does not appear for the ultraviolet radiation, the decay of which happens along one transition and is therefore characterized by a single decay rate. However, we cannot formulate the branching ratio in the form of Eq. (4.1); and instead, we characterize the spontaneous emission process

by the operational definition given by Eq. (4.2).

For optically thin samples and decays from common upper level, the equality between two definitions Eqs. (4.1) and (4.2), i.e. the equality between the ratio of line intensities and the ratio of the corresponding decay rates, points to the way of measurements of decay rates. Thus, from measurements of the intensity ratio of two lines, the ratio R and one of the spontaneous decay rates can be deduced knowing the other. Such spectroscopic technique is rather popular in plasma physics. Particularly attractive is the fact that the branching ratio is as immune to environmental conditions as the decay rate is. For instance, the ratio does not depend on the electron density and temperature. In the experiments of [81], it is reported that for some transitions the branching ratio becomes the function of density (concentration). They interpreted this observation as quenching of spontaneous-emission coefficients for visible transitions. Our study is devoted to formulation of the problem in quantum-optical terms, and our model is based on the five-level scheme (see Fig. 20), and the effect is caused by collision-induced quantum coherence between two upper levels.

The best way to formulate our main result is to compare two cases. The first one corresponds to no coherence between upper levels a and b. Then, the branching ratio for visible and ultraviolet transition found from the operational definition (4.2) reads

$$R = 2\frac{\gamma_{vis}}{\gamma_{UV}} \tag{4.3}$$

as found in the following sections. Here the difference in the factor of two from original definition (4.1) arises due to doubling the visible decay rate (here $\gamma_a = \gamma_b \equiv \gamma_{vis}$) by taking into account decays from both upper levels (with equal rates). In contrast, the rate on the ultraviolet transition is not doubled because the spontaneous decay originates from single level a. Apart from this factor, the equation (4.3) stands in

line with regular expectations. In particular, this result is unable to explain the concentration dependence of R reported in [81].

The second case realizes when the (maximal) coherence between levels a and b is induced by electron collisions. Then, as we shall show in the following sections, the branching ratio under steady-state conditions is given by

$$R = \gamma_{vis}\left(\frac{4}{r_e} + \frac{1}{r_{vis}}\right) = \frac{\gamma_{vis}}{N}\sqrt{\frac{\pi M}{kT}}\left(\frac{2e^{\frac{E_e}{kT}}}{\overline{k}_e} + \frac{e^{\frac{E_a}{kT}}}{2\overline{k}_{vis}}\right) \tag{4.4}$$

where, for simplicity, the result is evaluated in the limit of large pumping rates: $r_{vis}, r_e \gg \gamma_{vis}, \gamma_{UV}$; and k_i is the appropriate cross-sections of electronic excitation. Since all involved pumping rates depend on the electron concentration, the branching ratio also becomes concentration-dependent. The higher the concentration the faster the pumping rates and therefore the lower the branching ratio. This relation implies quenching of spontaneous emission on the visible transition.

In the following sections we shall show that the effect of quenching is explained by creation of the collision-induced (i.e. induced by pumping rate r_{vis}) dark state as a linear combination of upper states a and b. This dark state does not emit radiation and the more atoms we pump into this state the better suppression of spontaneous emission we observe. Indeed, as shown below, by pumping more atoms in the dark state via increasing r_e with concentration we achieve more efficient quenching. In contrast, the emission on the ultraviolet transition does not depend on the coherence between levels a and b and is linearly proportional to population of a level only. By formulating the branching ratio R, all common dependencies cancel out and only the purified asymmetry of responses on the visible and ultraviolet transitions is left. Here, the branching ratio shows up as a valuable measure of the coherence-induced quenching of spontaneous emission on the visible transition.

Overall, in this chapter we report the scheme with spontaneous emission can-

cellation resulted from incoherent pumping of atoms into the collision-induced dark state. As quantitative measure of the degree of the cancellation we propose to use the operational definition of the branching ratio given in Eq. (4.2). Our scheme provides a possible physical explanation for the quenching effects reported in [81].

B. Basic set of equations

We study the set of equations of motion governing temporal evolution of the density matrix elements for the five-level scheme shown in Fig. 20. The key ingredient of this scheme is the three-level V -type system consisting of two upper states $|a\rangle$, $|b\rangle$ connected to the lower state $|c\rangle$ by dipole allowed transitions. We first consider this three-level subsystem and then add two states $|d\rangle$ and $|e\rangle$. We assume that two transitions $|a\rangle - |c\rangle$ and $|b\rangle - |c\rangle$ have close transition frequencies and therefore upper states decay to same continuum of vacuum modes with decay constants γ_a and γ_b. These constants as well as details of the decay process follow from the Hamiltonian

$$V_\gamma = \hbar \sum_k g_k^{(a)} e^{i(\omega_{ac}-\nu_k)t} |a\rangle\langle c|\hat{a}_k + \hbar \sum_k g_k^{(b)} e^{i(\omega_{bc}-\nu_k)t} |b\rangle\langle c|\hat{a}_k + H.c. \tag{4.5}$$

describing interaction between the atom and the reservoir of vacuum oscillators, each of frequency ν_k (k here represents both the momentum and polarization of the vacuum mode). Here $g_k^{(a,b)}$ are the coupling constants between the k-th vacuum mode and the atomic transitions from $|a\rangle$ and $|b\rangle$ to $|c\rangle$. $\hat{a}_k(\hat{a}_k^\dagger)$ is the annihilation (creation) operator of a photon in the k-th vacuum mode, which obeys conventional bosonic commutation rule $[\hat{a}_k, \hat{a}_k^\dagger] = \delta_{kk'}$.

Electron collisions transfer atoms (also ions as in the plasma experiments in Ref. [81]) between states in the manner very much like that in the process of interaction with an optical field. As a consequence, the Hamiltonian appears in a similar form,

as

$$V_R = \wp_{ac}\Omega|a\rangle\langle c| + \wp_{bc}\Omega|b\rangle\langle c| + H.c. \tag{4.6}$$

In contrast to coherent optical fields, individual collisional events are not correlated with each other and therefore the effective field Ω is incoherent. Note that spectrum of this incoherent field is very broad so that it covers both upper levels simultaneously, and therefore one and the same field drives both transitions. These transitions are characterized by dipole matrix elements $\wp_{ac}$ and $\wp_{bc}$ and transition frequencies ω_{ac} and ω_{bc}. The incoherent field has δ-like correlations at different times, i.e.,

$$\langle \Omega^*(t)\Omega(t')\rangle = R\delta(t-t') \tag{4.7}$$

These correlations are not expected to cover the entire range of frequencies from $-\infty$ to $+\infty$. It is sufficient that they are at least approximately valid in the vicinity of both resonances and cover the frequency separation of two upper levels.

The total interaction picture Hamiltonian for the three-level subsystem is the sum of two terms introduced above,

$$H = V_\gamma + V_R \tag{4.8}$$

Derivation of equations of motion for the density matrix elements from the total Hamiltonian is a straightforward task. It is based on the scheme well developed in quantum optics, see for instance [82], where main ingredients are the Wigner-Weisskopf approximation and the generalized reservoir theory [83]. More details, particularly on the 6 system under consideration, can be found in our recent paper [84]. With this reference to prior works we skip the derivation and jump directly to

the equations of motion. They read

$$\dot{\rho}_{aa} = -(r_a + \gamma_a)\rho_{aa} + r_a\rho_{cc} - \frac{1}{2}p\sqrt{r_a r_b}(\rho_{ba} + \rho_{ab}) \tag{4.9}$$

$$\dot{\rho}_{bb} = -(r_b + \gamma_b)\rho_{bb} + r_b\rho_{cc} - \frac{1}{2}p\sqrt{r_a r_b}(\rho_{ba} + \rho_{ab}) \tag{4.10}$$

$$\dot{\rho}_{cc} = (r_a + \gamma_a)\rho_{aa} + (r_b + \gamma_b)\rho_{bb} - (r_a + r_b)\rho_{cc} + p\sqrt{r_a r_b}(\rho_{ba} + \rho_{ab}) \tag{4.11}$$

$$\dot{\rho}_{ab} = -\frac{1}{2}(r_a + r_b + \gamma_a + \gamma_b)\rho_{ab} - i\Delta\rho_{ab} + \frac{1}{2}p\sqrt{r_a r_b}(2\rho_{cc} - \rho_{aa} - \rho_{bb}) \tag{4.12}$$

$$\dot{\rho}_{ca} = -\frac{1}{2}(2r_a + r_b + \gamma_a)\rho_{ca} - \frac{1}{2}p\sqrt{r_a r_b}\rho_{cb} \tag{4.13}$$

$$\dot{\rho}_{cb} = -\frac{1}{2}(2r_b + r_a + \gamma_b)\rho_{cb} - \frac{1}{2}p\sqrt{r_a r_b}\rho_{ca} \tag{4.14}$$

Here $r_{a,b} \equiv 2(\wp_{ac,bc}^2/\hbar^2)R$ are pumping rates of atoms to upper states $|a\rangle$ and $|b\rangle$ induced by collisions with electrons, see Fig. 20. Detuning $\Delta = \omega_{ac} - \omega_{bc}$ is supposed to be small as compared to the optical frequency and should be of the order of pumping rates r_a or r_b or less in order to make quantum interference effects observable.

Terms containing products of pumping rates appear due to the interference of two optical transitions which is induced by collisions with electrons. These terms are central to our discussion. In order to emphasize the role of this collision-induced interference, we assume that decay channels do not interfere. The interference terms are accompanied by the p factor. This factor is the normalized scalar product of corresponding dipole matrix elements:

$$p = \frac{\wp_{ac} \cdot \wp_{bc}}{|\wp_{ac}\wp_{bc}|} \tag{4.15}$$

According to its definition, the alignment factor takes the value equal to 1 for parallel dipole moments, -1 for antiparallel, and 0 for orthogonal. Intermediate values on $[-1, 1]$ segment are also possible. Maximal coherence corresponds to parallel or antiparallel dipole moments, while zero coherence corresponds to orthogonal dipole moments. These two extremes of maximal and minimal coherence deserve special

attention.

It is not difficult to proceed with modeling the system shown in Fig. 20 and supplement the three-level subsystem with two additional levels. For further considerations we shall need only equations for populations and one equation for the polarization on $|a\rangle - |d\rangle$ transition. The upper state $|e\rangle$ is subject to decay with rate γ_e and pumping from state $|c\rangle$ by electronic collisions with rate r_e. So, for the population we immediately obtain

$$\dot{\rho}_{ee} = r_e(\rho_{cc} - \rho_{ee}) - 2\gamma_e\rho_{ee} \tag{4.16}$$

Of course, we could derive this equation from first principles by writing the Hamiltonian of interaction of the atom with the continuum of quantum oscillators to model the decay and interaction with the incoherent electron field to model the pumping process. Since no interference effects are expected on this transition, this derivation is no more than a trivial exercise. The intuitive appearance of this equation stays in contrast to the detailed consideration of the V -type subsystem where the nontrivial appearance of interference terms requires cautious analysis.

Similar equation can be written for the lowest state of the system, $|d\rangle$. Here the decay with rate γ_{UV} from $|a\rangle$ state pumps the $|d\rangle$ state. The electron pumping is modeled by rate r_{UV}. So, in accordance with the picture in Fig. 20 we write

$$\dot{\rho}_{dd} = r_{UV}(\rho_{cc} - \rho_{dd}) + \gamma_{UV}\rho_{aa} \tag{4.17}$$

We now complete the set of equations by writing the equation of motion for the polarization on $|a\rangle - |d\rangle$ transition:

$$\dot{\rho}_{ad} = -\frac{1}{2}(\gamma_{UV} + r_{UV})\rho_{ad} \tag{4.18}$$

We can also write down equations of motion for the other polarizations involving

states $|e\rangle - |d\rangle$. However, we do not do this because these equations are not used in further analysis. For more general considerations, if necessary, they can be composed by following directly the picture in Fig.20. Note that no interference terms appear.

To complete the model we should account for decays and pumpings between the V-subsystem and $|d\rangle$ and $|e\rangle$ states. The subset of equations (4.9)-(4.14) are modified in the following way. There is one incoming term for the population of $|b\rangle$ state: $+\gamma_e\rho_{ee}$. One incoming and one outcoming term for ρ_{aa} : $+\gamma_e\rho_{ee}$ and $-\gamma_{UV}\rho_{aa}$. For ρ_{cc} we get two additional pumping terms, $+r_e(\rho_{ee} - \rho_{cc})$ and $+r_{UV}(\rho_{dd} - \rho_{cc})$. The equation of motion for the two-photon coherence ρ_{ab} should be supplemented with decay term $\frac{1}{2}\gamma_{UV}\rho_{ab}$. One-photon polarization ρ_{ac} also decays faster due to additional decay term $\frac{1}{2}(r_e + r_{UV} + \gamma_{UV})\rho_{ac}$. Finally, in the equation for ρ_{bc} we should also write additional decay term $\frac{1}{2}(r_e + r_{UV})\rho_{bc}$. In the next section we summarize all these changes and after implementing a few simplified assumptions write down modified equations.

C. Dressed-state analysis

In this section we consider properties of the V-type subsystem $|a\rangle - |b\rangle - |c\rangle$ in the dressed-state picture. Before doing this we first prefer to make some simplifications. Assume equal dipole moments on $|a\rangle - |c\rangle$ and $|b\rangle - |c\rangle$ 8 transitions: $\wp_{ac} = \wp_{bc}$. This assumption immediately yields the equality of decay constants: $\gamma_a = \gamma_b$. We also get equal pumping rates, $r_a = r_b$. Also, let the two transitions have equal frequencies, so that two-photon detuning Δ is zero.

The upper level $|e\rangle$ is auxilary with respect to the rest of the system. It serves to model the external pumping of two upper levels of the V -subsystem. In plasmas this pumping is due to thermal redistribution of population from all levels which are higher

with respect to $|a\rangle$ and $|b\rangle$. In order to accurately account for details of this process we would have to consider a particular level scheme for a given atom/ion. However, our immediate goal is not the one-to-one description of a particular experiment but rather the proof-of-principle theoretical study of relevant coherent effects. Guided by simplicity we eliminate level $|e\rangle$ from our five-level scheme. For that purpose, we assume fast decay rate γ_e with respect to pumping rate r_e. Then, from the equation (4.16) we can write for the population ρ_{ee} in steady-state:

$$\rho_{ee} \approx \frac{r_e}{\gamma_e}\rho_{cc} \tag{4.19}$$

With these simplifications in effect and additional terms from the discussion in the end of the previous section, equations (4.9)-(4.14) for the V -subsystem become

$$\dot{\rho}_{aa} = -(r_{vis} + \gamma_{vis} + \gamma_{UV})\rho_{aa} + (r_{vis} + \frac{r_e}{2})\rho_{cc} - pr_{vis}\rho_{ab} \tag{4.20}$$

$$\dot{\rho}_{bb} = -(r_{vis} + \gamma_{vis})\rho_{bb} + (r_{vis} + \frac{r_e}{2})\rho_{cc} - pr_{vis}\rho_{ab} \tag{4.21}$$

$$\dot{\rho}_{cc} = (r_{vis} + \gamma_{vis})(\rho_{aa} + \rho_{bb}) - (2r_{vis} + r_e + r_{UV})\rho_{cc} + 2pr_{vis}\rho_{ab} + r_{UV}\rho_{dd} \tag{4.22}$$

$$\dot{\rho}_{ab} = -(r_{vis} + \gamma_{vis} + \frac{\gamma_{UV}}{2})\rho_{ab} + \frac{1}{2}pr_{vis}(2\rho_{cc} - \rho_{aa} - \rho_{bb}) \tag{4.23}$$

with new notations: $\gamma_a = \gamma_b \equiv \gamma_{vis}$ and $r_a = r_b \equiv r_{vis}$. Here we write down only equations relevant for the study in this section. Equations for one-photon polarizations ρ_{ca} and ρ_{cb} will be considered in the next section.

Coherent effects in the V-subsystem appear due to the interference of pumping channels along $|a\rangle - |c\rangle$ and $|b\rangle - |c\rangle$ transitions. Actually, it is the same (incoherent) pumping process that drives both transitions. The presence of the coherence shows up in most natural way in the dressed-state basis. Here, the pumping field dresses

atomic states $|a\rangle$ and $|b\rangle$ yielding the collision-induced dark state:

$$|D\rangle = \frac{\sqrt{r_b}|a\rangle - \sqrt{r_a}|b\rangle}{\sqrt{r_a + r_b}} \tag{4.24}$$

and its orthogonal partner - bright state:

$$|B\rangle = \frac{\sqrt{r_a}|a\rangle + \sqrt{r_b}|b\rangle}{\sqrt{r_a + r_b}} \tag{4.25}$$

Here we formulate the dark and bright states for general relationship between pumping rates to emphasize that our treatment is valid beyond the simplification assumption of equal dipole moments. When $r_a = r_b$ the expressions become

$$|D\rangle = \frac{1}{\sqrt{2}}(|a\rangle - |b\rangle) \tag{4.26}$$

$$|B\rangle = \frac{1}{\sqrt{2}}(|a\rangle + |b\rangle) \tag{4.27}$$

In the following we shall see that the bright state has direct relationship to the rate of correlated spontaneous emission from bare upper states $|a\rangle$ and $|b\rangle$.

Since Schrödinger description is impossible for the given scheme of decay and pumping rates, the formulation of equations of motion in terms of the dressed variables requires introduction of corresponding density matrix elements. They are

$$\rho_{DD} = \frac{1}{2}(\rho_{aa} + \rho_{bb} - 2\rho_{ab}) \tag{4.28}$$

$$\rho_{BB} = \frac{1}{2}(\rho_{aa} + \rho_{bb} + 2\rho_{ab}) \tag{4.29}$$

$$\rho_{DB} = \frac{1}{2}(\rho_{aa} - \rho_{bb}) \tag{4.30}$$

where we assume definitions of the dark and bright states given in equations (4.26) and (4.27) and real two-photon polarization ρ_{ab}. The last is valid assumption for zero two-photon detuning. If necessary, it is rather straightforward to derive the density matrix elements for general relationship between pumping rates and for nonzero two-

photon detuning.

Given equations of motion in bare-states basis, (4.20), (4.21) and (4.23), and dressed-states definitions (4.28)-(4.30) for the density matrix elements, we reformulate these equations as

$$\dot{\rho}_{DD} = -\gamma_{vis}\rho_{DD} - \frac{\gamma_{UV}}{2}(\rho_{DD} + \rho_{DB}) + r_e\rho_{cc} \tag{4.31}$$

$$\dot{\rho}_{BB} = -(2r_{vis} + \gamma_{vis})\rho_{BB} - \frac{\gamma_{UV}}{2}(\rho_{BB} + \rho_{DB}) + (2r_{vis} + r_e)\rho_{cc} \tag{4.32}$$

$$\dot{\rho}_{DB} = -(r_{vis} + \gamma_{vis} + \frac{\gamma_{UV}}{2})\rho_{DB} - \frac{1}{4}\gamma_{UV}(\rho_{DD} + \rho_{BB}) \tag{4.33}$$

Our ultimate goal is the comparison of intensities of spontaneous emissions on the visible transition on one hand and on the ultraviolet transition on the other. As we shall derive in the next section, these intensities are linearly proportional to the population of $|B\rangle$ state and $|a\rangle$ state, correspondingly. Both these populations can be obtained from the solution of equations (4.31)-(4.33) and inverted conversion formulas (4.28)-(4.30). It is not difficult to obtain exact steady-state solutions for all three dressed-states density matrix elements in above equations. However, we prefer to make yet another simplification in order to bring physics in the clearest possible form.

We assume that pumping rates are much faster than decay processes, particularly faster than the fastest decay rate γ_{UV}. Note that the spontaneous emission rate γ_{UV} is two orders of magnitude greater than decay rate γ_{vis} on the visible transition. Clearly, this difference is attributed to the cubic dependence of spontaneous decay rates on the transition frequency. In its turn, the high efficiency of pumping processes arises from frequent collisions of ions with free electrons (note that the electron concentration N_e exceeds the value of $10^{18}cm^{-3}$). Finally, we formulate our assumption in the form of

strong inequality

$$r_{vis}, r_e \gg \gamma_{UV}, \gamma_{vis} \tag{4.34}$$

This inequality is the key to understanding the effect of suppression of spontaneous emission on the visible transition. This understanding comes from the analysis of the equation (4.31). We shall see that more atoms in the dark state makes the emission weaker. The first two terms in equation (4.31) stand for the depletion of the dark state and are therefore undesirable for our purposes. [Note that steady-state polarization ρ_{DB} contributes as little as $(\gamma_{UV}/r_{vis})\rho_{DD}$.] This depletion is counterbalanced by the gain associated with the last term. The large value of this term requires fast pumping rate that is guaranteed by inequality (4.34).

With inequality (4.34) we get approximate solutions of equations (4.31)-(4.33). They are

$$\rho_{DD} \approx \frac{r_e}{\gamma_{UV}}\rho_{cc} \tag{4.35}$$

$$\rho_{BB} \approx (1 + \frac{r_e}{4r_{vis}})\rho_{cc} \tag{4.36}$$

$$\rho_{DB} \approx \frac{r_e}{r_{vis}}\rho_{cc} \tag{4.37}$$

where we also used $\gamma_{UV} \gg \gamma_{vis}$. All these solutions are expressed in terms of ρ_{cc} which remains unknown quantity until we solve all equations of motion for the closed five-level system. However, the explicit knowledge of ρ_{cc} is not necessary for our study.

Solution (4.35) shows that the dark state is populated only due to the pumping via auxiliary upper state $|e\rangle$. By comparing solutions given by formulas (4.35) and (4.36) and using inequality (4.34), we conclude that $\rho_{DD} \gg \rho_{BB}$, so that the population of upper states $|a\rangle$ and $|b\rangle$ is dominantly concentrated in the dark state. This asymmetry means that most atoms are trapped in the non-emitting state $|D\rangle$. As we shall see shortly, the spontaneous emission on the visible transition is proportional

to ρ_{BB}; and therefore basing on the just derived strong inequality $\rho_{DD} \gg \gamma_{BB}$, we conclude that the emission is strongly suppressed. This suppression is to be put in comparison with the regular (unsuppressed) emission on the ultraviolet transition, which is regulated by the amount of population in the $|a\rangle$ state. Overall, the degree of suppression is quantitatively estimated by the corresponding branching ratio, as the ratio of two emissions, see Eq. (4.2) and derivations in the next section.

The population of the $|a\rangle$ state as well as ρ_{bb} and ρ_{ab} can be found by inverting definitions (4.28)-(4.30). So, in terms of bare states we get

$$\rho_{aa} = \frac{1}{2}(\rho_{BB} + \rho_{DD} + 2\rho_{DB}) \approx \frac{r_e}{2\gamma_{UV}}\rho_{cc} \tag{4.38}$$

$$\rho_{bb} = \frac{1}{2}(\rho_{BB} + \rho_{DD} - 2\rho_{DB}) \approx \frac{r_e}{2\gamma_{UV}}\rho_{cc} \tag{4.39}$$

$$\rho_{ab} = \frac{1}{2}(\rho_{BB} - \rho_{DD}) \approx -\frac{r_e}{2\gamma_{UV}}\rho_{cc} \tag{4.40}$$

This state is the state of maximal coherence in the sense that $|\rho_{ab}| \approx \sqrt{\rho_{aa}\rho_{bb}}$. This coherence is of collisional nature and its high degree is the reflection of the high efficiency of the pumping mechanism (r_{vis}). So, we deal here with almost pure states.

In this section we performed the analysis of the V -subsystem in terms of dressed states and introduced the important approximation (4.34) which is the key to understanding of the effect of suppression of spontaneous emission on the visible transition. In the next section we proceed with derivation of the emission rates on visible and ultraviolet transitions and put them in comparison in terms of the branching ratio defined via Eq. (4.2).

D. Spontaneous emission spectra

The idea is to calculate the spectrum $S_{vis}(\omega)$ of spontaneously emitted photons on the visible transition, i.e. through $|a\rangle - |c\rangle$ and $|b\rangle - |c\rangle$ channels. Then, we similarly

calculate the ultraviolet spectrum $S_{UV}(\omega)$ of photons emitted in the $|a\rangle - |d\rangle$ channel. Integrating these two spectra over the frequencies in the vicinity of the corresponding emission peaks and normalizing to the energy of one photon, we thus obtain two spectral-line intensities

$$I_{vis} = (\hbar\omega_{vis})^{-1} \int d\omega S_{vis}(\omega) \tag{4.41}$$

$$I_{UV} = (\hbar\omega_{UV})^{-1} \int d\omega S_{vis}(\omega) \tag{4.42}$$

Taking the ratio of these intensities we formulate the branching ratio defined in Eq. (4.2), finally in terms of relevant pumping rates and decay constants.

Spontaneous emission spectrum of a two-level atom became already a textbook subject in quantum optics, see for instance [82]. Here the characteristic three-peak spectrum emerges in an elegant way as a result of application of the quantum regression theorem. The latter allows us to express the two-time correlation function in terms of one-time correlation functions and thereby significantly simplifies the calculation procedure.

Spontaneous emission spectra of coherently driven three and more level atoms were the subject of interest in numerous papers, see for instance [85]. Again, the quantum regression theorem is of great help. However, even in the case of three levels the calculation procedure quickly becomes cumbersome and requires numerical analysis on the final stage. Details can be found in the original paper [85]. In our case the system is driven by an incoherent field that makes the situation a little simpler. Furthermore, applying the so far discussed approximations and simplifications, we can make the problem even analytically tractable with transparent final result. We even bypass the direct application of the quantum regression theorem.

First, we take the definition of the spectrum (valid for stationary processes) as the Fourier transform of the autocorrelation function of the second order of the scattered

electric field:

$$S(\omega) = \frac{1}{\pi} Re \int_0^\infty d\tau e^{-i\omega\tau} \langle E^-(r,t) \cdot E^+(r,t+\tau) \rangle \tag{4.43}$$

This autocorrelation function is simply related to the normally-ordered product of polarizations taken at instants of time separated by a positive time delay τ. This relationship follows from the well-known formula

$$E^+(r,t) = -\frac{\omega_0^2}{4\pi\varepsilon_0 c^2 r} \mathbf{n} \times (\mathbf{n} \times \mathbf{d}) \mathbf{P}^{(+)}(t - r/c) \tag{4.44}$$

connecting the electric field $\mathbf{E}^{(+)}$ with polarization $\mathbf{P}^{(+)}$. Here, $\mathbf{n}$ is the unit vector in the direction of observation, $\mathbf{d}$ is the unit vector along the atomic dipole moment, $\mathbf{r}$ is the observation point, measured from the position of the atom, and ω_0 is the polarization frequency. More details can be found, for instance in Ref. [85]. The resultant formulas are

$$S_{vis}(\omega) = \frac{C\omega_{vis}^4}{\pi} Re \int_0^\infty d\tau e^{-i\omega\tau} \langle P_{vis}^-(t) \cdot P_{vis}^+(t+\tau) \rangle \tag{4.45}$$

$$S_{UV}(\omega) = \frac{C\omega_{UV}^4}{\pi} Re \int_0^\infty d\tau e^{-i\omega\tau} \langle P_{UV}^-(t) \cdot P_{UV}^+(t+\tau) \rangle \tag{4.46}$$

Here C is an unimportant constant, same for both transitions. $P_{vis}^{(-)}$ and $P_{vis}^{(+)}$ ($P_{UV}^{(-)}$and $P_{UV}^{(+)}$) are negative and positive frequency parts of the polarization induced on the visible(ultraviolet) transition. According to our scheme they are defined as

$$P_{vis}^-(t) = \wp_{ac}\sigma_{ac}(t) + \wp_{bc}\sigma_{bc}(t) \tag{4.47}$$

$$P_{vis}^+(t+\tau) = \wp_{ca}\sigma_{ca}(t+\tau) + \wp_{cb}\sigma_{cb}(t+\tau) \tag{4.48}$$

Similarly we define the negative- and positive-frequency parts of the polarization on the ultraviolet transition:

$$P_{UV}^-(t) = \wp_{ad}\sigma_{ad}(t) \tag{4.49}$$

$$P^{+}_{UV}(t+\tau) = \wp_{da}\sigma_{da}(t+\tau) \tag{4.50}$$

In the following we assume $\wp_{ac} = \wp_{ca} = \wp_{bc} = \wp_{cb}$ and $\wp_{ad} = \wp_{da}$.

Operators of atomic transitions σ_{ij} are defined in usual way: $\sigma ij = |i\rangle\langle j|$. They are particularly relevant for the calculation of multi-time correlation functions. Note that these quantities are quantum-mechanical operators. Their quantum-mechanical average has simple relation to the elements of the density matrix, namely

$$\begin{aligned} \langle\sigma_{ij}(t)\rangle &= Tr[U^{+}(t)\sigma_{ij}(0)U(t)\rho(0)] \\ &= Tr[\sigma_{ij}(0)U(t)\rho(0)U^{+}(t)] \\ &= Tr[\sigma_{ij}(0)\rho(t)] \end{aligned} \tag{4.51}$$

Since we need to calculate two-time correlation functions, it is instructive to write down equations of motion for relevant operators and then find solutions to the initial-value problem. The form of these equations coincide with the equations of motion for respective density matrix elements. This can be checked by direct derivation from the Heisenberg equation of motion with the Hamiltonian [77]. Thus we get

$$\sigma_{ac} = -\frac{1}{2}(3r_{vis} + r_{UV} + r_e + \gamma_{vis} + \gamma_{UV})\sigma_{ac} - \frac{1}{2}r_{vis}\sigma_{bc} \tag{4.52}$$

$$\sigma_{bc} = -\frac{1}{2}(3r_{vis} + r_{UV} + r_e + \gamma_{vis})\sigma_{bc} - \frac{1}{2}r_{vis}\sigma_{ac} \tag{4.53}$$

$$\sigma_{ad} = -\frac{1}{2}(r_{vis} + r_{UV} + r_e + \gamma_{vis} + \gamma_{UV})\sigma_{ad} \tag{4.54}$$

where we used the assumption $r_a = r_b \equiv r_{vis}$. Note that $\sigma_{ji} = \sigma^{\dagger}_{ij}$ and the equations of motion for the conjugate operators arise by taking the Hermite conjugate of the right-hand sides of Eqs. (4.52)-(4.54). The above equations form the closed system and allow simple solutions. These solutions acquire even simpler form when we apply

our key inequality (4.34). Thus, for the quantities of interest we get

$$\sigma_{ca}(t+\tau) + \sigma_{cb}(t+\tau) = e^{-\frac{1}{2}r_0\tau}[\sigma_{ca}(t) + \sigma_{cb}(t)] \tag{4.55}$$

$$\sigma_{da}(t+\tau) = e^{-\frac{1}{2}(r_{UV}+r_{vis})\tau}\sigma_{da}(t) \tag{4.56}$$

where $r_0 \equiv (2r_{vis} + r_{UV} + r_e)$.

Everything is ready for the formulation of the desired result. After substituting solution (4.55) in the expression (4.48) and correspondingly (4.56) in (4.50), the two-time correlation functions of the polarizations read

$$\langle P^-_{vis}(t) \cdot P^+_{vis}(t+\tau)\rangle = \wp^2_{ac} e^{-r_0\tau}\langle(\sigma_{aa}(t) + \sigma_{bb}(t) + \sigma_{ab}(t) + \sigma_{ba}(t)\rangle \tag{4.57}$$

$$\langle P^-_{UV}(t) \cdot P^+_{UV}(t+\tau)\rangle = \wp^2_{ad} e^{-(r_{UV}+r_{vis})\tau}\langle\sigma_{aa}(t)\rangle \tag{4.58}$$

The Fourier transform of the above expressions converts the exponential decays in time to the Lorentzian spectra in frequency:

$$S_{vis}(\omega) = \frac{C\omega^2_{vis}\wp^2_{ac}}{\pi}\frac{r_0}{\omega^2 + r_0^2}2\rho_{BB}(t) \tag{4.59}$$

$$S_{UV}(\omega) = \frac{C\omega^2_{UV}\wp^2_{ad}}{\pi}\frac{r_{UV} + r_{vis}}{\omega^2 + (r_{UV} + r_{vis})^2}\rho_{aa}(t) \tag{4.60}$$

Here we take only the real part of the integral and use the rule (4.51) for calculating quantum-mechanical averages, and also the definition of the population of the bright state (4.29). Note also the equality $\rho_{ab} = \rho_{ba}$ valid for the zero value of the two-photon detuning, which is the case considered here.

Note here that it may seem that the thus obtained spectra can, in principle, become a function of time, copying the time dependence of populations ρ_{BB} and ρ_{aa}. This dependence is a signature of a nonstationary process. Therefore the spectrum of these solutions is to be defined not by Eq. (4.43) but with the more general formula which is derived and discussed for instance in Ref. [82]. However, in our

case the interest is in stationary emission corresponding to steady-state solutions for ρ_{BB} and ρ_{aa}. Therefore, ρ_{BB} and ρ_{aa} become time independent. In Fourier space they are simply two stationary Lorentzian peaks. Spectral-line intensities follow as the frequency integral over these peaks:

$$I_{vis} = \hbar^{-1} C \omega_{vis}^3 \wp_{ac}^2 2\rho_{BB} \tag{4.61}$$

$$I_{UV} = \hbar^{-1} C \omega_{UV}^3 \wp_{ad}^2 \rho_{aa} \tag{4.62}$$

The branching ratio is the ratio of two above quantities, as regulated by definition (4.2):

$$R = \frac{\gamma_{vis}}{\gamma_{UV}} \frac{2\rho_{BB}}{\rho_{aa}} \tag{4.63}$$

where we used the definition of the spontaneous decay constant

$$\gamma_{vis} = \frac{1}{4\pi\varepsilon_0} \frac{4\omega_{vis}^3 \wp_{ac}^2}{3\hbar c^3} \tag{4.64}$$

and similar formula for the ultraviolet transition, and canceled out common prefactors.

This ratio is the main formula of our chapter. It reflects the role of coherent effects in the spontaneous emission along the visible transition. A small population in the bright state on the background of relatively strongly populated $|a\rangle$ state implies the suppression of the spontaneous decay. Such asymmetry becomes possible only when the coherence ρ_{ab} between the two upper states $|a\rangle$ and $|b\rangle$ acquires an appreciable value. Here, the coherence is induced by collisions and its large value is guaranteed by the inequality (34), which means that decay processes destroying the coherence are of little importance. Quantitatively, the degree of the suppression is related to the value of R in absence of the interference terms which becomes simply the double ratio of decay constants, as we show below.

E. Suppression of the spontaneous decay

The branching ratio given by Eq. (4.63) is now the subject of the analysis with respect to the experimental observations in Ref. [81]. First of all we use steady-state values of populations given by solutions (4.36) and (4.38) in Eq. (4.63) and obtain

$$R = \gamma_{vis} \left(\frac{4}{r_e} + \frac{1}{r_{vis}} \right) \tag{4.65}$$

The common factor ρ_{cc} has been canceled out. According to the experimental observations in Ref. [81], the branching ratio was measured as the function of electron density. One order of magnitude increase in the electron density resulted in one order of magnitude decrease in the branching ratio. Let us see how such dependence emerges from the above equation.

The decay constant γ_{vis} depends nontrivially on the frequency and the dipole moment, see Eq. (4.64). Within the range of change of the experimental conditions, no dependence of the transition frequency (i.e., no line shift) on electron density was found. Some theoretical efforts were made in Ref. [86] to take into account the effect of the screening of the atomic potential by the surrounding plasma. This effect can, in principle, modify the Coulomb field experienced by the valence electron and, thus, significantly change the transition probability (i.e. dipole moment). However, this change becomes of an appreciable value only for concentrations much higher than that used in the experiment. So, we conclude that no change takes place in the value of γ_{vis} when concentration varies.

The observed changes of the branching ratio R in Ref. [81] can be attributed mainly to the dependence of collisional rates r_e and r_{vis} (and, of course r_{UV}) on the density of free electrons. Apparently the higher the density the more frequently the collision events occur and therefore the larger the rates. More precisely, we assume

linear dependence of the collisional rates on the concentration ($r_i \propto N$) and write for a constant electron temperature

$$r_i(N) = k_i N \tag{4.66}$$

where $i = e, vis, UV$, and k_i is the proportionality coefficient. Typical range of concentrations where the effect occurs covers the region $10^{18} - 10^{19} cm^{-3}$. Applying dependences given by Eq. (4.66) to Eq. (4.65), we perform simulation and present obtained results in Fig. 21. We thus illustrate main result of our study - the sensitive dependence of the branching ratio on the concentration. The range of the change is of the same order as was observed in the experiments.

For completeness we analyze the dependence of the collisional rates (and therefore, the branching ratio) on the electron temperature of plasma. This dependence, even when present, cannot be deduced from the experiments in Ref. [81] where the electron temperature was estimated as constant under operating conditions and equal to $\approx 5eV$. However, in the set of related experiments on measurements of the branching ratio in high-density plasmas of CIII performed in a later work in Ref. [87], the temperature varied considerably and, therefore, we can expect a well pronounced dependence of the branching ratio on the temperature. Thus for the concentration $0.7 \times 10^{18} cm^{-3}$, the temperature was 5.7 eV; while for higher concentration $2.6 \times 10^{18} cm^{-3}$, the temperature increased to $9.3eV$.

It is instructive to analyze the simultaneous electron density and temperature dependences. Free electrons in plasmas obey the classical Boltzmann distribution thus the number of particles dN (in a unit volume) within the range of energies $E + dE$ yields

$$dN = N\frac{2}{\sqrt{\pi}}\frac{1}{(kT)^{3/2}}e^{-\frac{E}{kT}}\sqrt{E}dE \tag{4.67}$$

So, for collisional rates we can write

$$r_i(N,T) = 2N\overline{k}_i\sqrt{\frac{2kT}{\pi M}}e^{-\frac{E_i}{kT}} \tag{4.68}$$

where $\overline{k}_i$ is a cross-section. Then the coefficient k_i is given by

$$k_i = 2\overline{k}_i\sqrt{\frac{2kT}{\pi M}}e^{-\frac{E_i}{kT}} \tag{4.69}$$

The branching ratio was measured in Ref. [87] for five concentration/temperature points.

F. Simulation results

For purposes of plasma diagnostics, we do or do not take into account the coherent effects due to electron impacts, depending on the relative orientation of the dipole moments of optical and UV transitions.

Numerical simulations are done based on Eqs. (4.72-4.77). Here we assume that $\gamma_{vis} = 1$, so that all the other parameters are normalized by γ_{vis}. The collision-induced incoherent pumping rates are dependent on electron density; here we use $r_{UV} = 0.001 \times N_e$, $r_e = 0.1 \times N_e$, and $r_v = 0.3 \times N_e$. We considered three different UV decay rates with $\gamma_{UV} = 0.1, 1, 5$ to investigate the dependence of branching ratio on electron density.

Fig.21.(a) corresponds to small UV decay rate $\gamma_{UV} = 0.1\gamma_{vis}$. Fig.21.(b,c) correspond to larger UV decay rate $\gamma_{UV} = 1, 5$ respectively. In each figure, the top red curve is for $p = 1$, the bottom blue curve is for $p = -1$, and the dashed line is for $p = 0$.

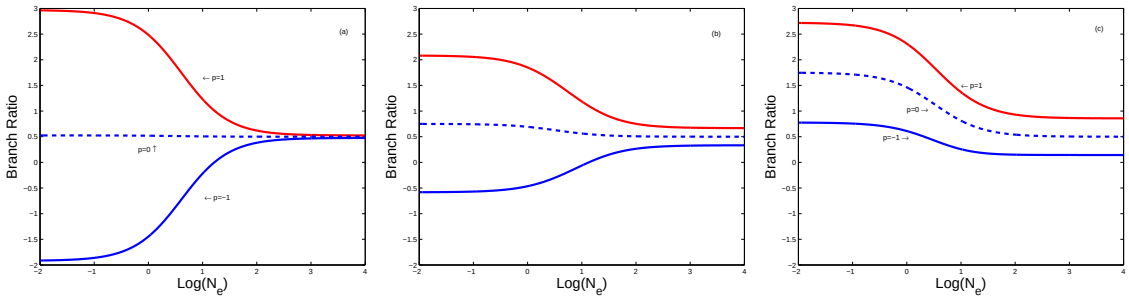

Fig. 21. The dependence of the branching ratio on logarithm of electron density. (a) For $\gamma_{uv} = 0.1\gamma_{vis}$, (b) For $\gamma_{uv} = \gamma_{vis}$,(c) For $\gamma_{uv} = 5\gamma_{vis}$. Three lines in each figure correspond to $p = 1, 0, -1$.

Through these nine cures, we notice that, at large electron density, the dependence of the branching ratio on density for different p factors behave in a similar way and trend to 0.5. In the special case with $p = 0$, this process gets to limit much more quickly. It is also clear that with larger UV decay rate, the dependence of the branching ratio on density for different p factors also behaves very similarly, but at a lower decay rate. At both sides of the extremely low or high electron density, there clearly limits. Outside this range, the electron density has no effect on the branching ratio.

Obvious conclusion from the comparison of curves is that the increase of temperature greatly suppresses variations in the branching ratio with concentration. The relatively small slope of the curve could be the reason or one of the reasons that yielded the very weak concentration dependence and led the experimenters in Ref. [87] to the conclusion of the absence of the dependence of the branching ratio on the concentration.

We thus complete the comparison with the experiments. On our way to the main result expressed by formula (4.65) we made two important assumptions. One is the condition of maximal coherence. The other is the domination of collisional rates over

all relevant decays, see Eq. (4.34). It is instructive now to see what happens if we relax the first assumption and consider the opposite case - the case of no coherence. Simply set p factor to zero; that is equivalent to setting $\rho_{ab} = 0$ (at least in the steady-state). Given inequality (4.34), two upper states $|a\rangle$ and $|b\rangle$ are populated equally in steady state. In the case of no coherence, the population of the bright state is simply one half of the sum of ρ_{aa} and ρ_{bb}. So, we get

$$\rho_{aa} \approx \rho_{BB} \approx (1 + \frac{r_e}{2r})\rho_{cc} \tag{4.70}$$

With these solutions in Eq. (4.63), we finally obtain

$$R \approx 2\frac{\gamma_{vis}}{\gamma_{UV}} \tag{4.71}$$

for the branching ratio for the visible and ultraviolet transitions in the case of no coherence between two upper states $|a\rangle$ and $|b\rangle$. This value is considerably larger than the branching ratio obtained for the case of maximal coherence, see Eq. (4.65). Moreover, this value does not depend on collisional rates and therefore on concentration. The comparison of branching ratios calculated for these two cases demonstrates the key role of coherence in interpreting experimental results obtained in Ref. [81].

G. Analytical solutions

Indeed, the set of equaitons is the following

$$\dot{\rho_a} = -(r_v + \gamma_v + r_{uv} + \gamma_{uv})\rho_a + r_v\rho_c + r_{uv}\rho_d + \gamma_e\rho_e - Pr_v\rho_{ab} \tag{4.72}$$

$$\dot{\rho_b} = -(r_v + \gamma_v)\rho_b + r_v\rho_c + \gamma_e\rho_e - Pr_v\rho_{ab} \tag{4.73}$$

$$\dot{\rho_c} = (r_v + \gamma_v)(\rho_a + \rho_b) - 2r_v\rho_c - r_e\rho_c + r_e\rho_e + 2Pr_v\rho_{ab} \tag{4.74}$$

$$\dot{\rho_{dd}} = r_{uv}(\rho_{aa} - \rho_{dd}) + \gamma_{uv}\rho_{aa} \tag{4.75}$$

$$\dot{\rho_e} = r_e(\rho_c - \rho_e) - 2\gamma_e\rho_e \tag{4.76}$$

$$\dot{\rho_{ab}} = -(r_v + g_v + g_{uv}/2)\rho_{ab} + \frac{1}{2}Pr_v(2\rho_c - \rho_a - \rho_b) \tag{4.77}$$

From Eq. (4.75),we obtain

$$\rho_d = \frac{r_{uv} + \gamma_{uv}}{r_{uv}}\rho_a = R_{da}\rho_a \tag{4.78}$$

And from Eq. (4.76), we get

$$\rho_e = \frac{r_e}{r_e + 2\gamma_e}\rho_c = R_{ec}\rho_c \tag{4.79}$$

Subtract Eq. (4.73) from Eq. (4.72), and by exploiting Eq. (4.75), we obtain that

$$\rho_a = \rho_b \tag{4.80}$$

From Eq. (4.77), we obtain

$$\rho_{ab} = \frac{Pr_v}{\Gamma_{ab}}(\rho_c - \rho_a) \tag{4.81}$$

where

$$\Gamma_{ab} = r_v + g_v + g_{uv}/2 \tag{4.82}$$

Substituted Eq.(4.81)into Eq.(4.74), and by exploiting Eq. (4.80) and Eq. (4.79), we obtain

$$\rho_c = R_{ca}\rho_a \tag{4.83}$$

where we introduce

$$R_{ca} = \frac{2(r_v + g_v - P^2r_v^2/\Gamma_{ab})}{2r_v + r_e - r_eR_{ec} - 2P^2r_v^2/\Gamma_{ab}} \tag{4.84}$$

Here we can use the conservation of the electron number. Suppose that the total

number of electrons in all levels is

$$\rho_a + \rho_b + \rho_c + \rho_d + \rho_e = 1 \tag{4.85}$$

Thus we get

$$\rho_a = \frac{1}{2 + R_{ca} + R_{da} + R_{ec}R_{ca}} \tag{4.86}$$

By exploiting the relationships of density between different levels, we can find each level's density.

It is known that the density of the bright state is defined as

$$\rho_{BB} = \rho_a + \rho_b + 2\rho_{ab} \tag{4.87}$$

and the definition of the branch ratio is

$$R \approx \frac{\rho_{BB}}{\rho_a} \tag{4.88}$$

By using all the results we have obtained, we finally get the expression of the branch ratio

$$R = 2 + \frac{2Pr_v}{\Gamma_{ab}}(2R_{ca} - 1) \tag{4.89}$$

The branching ratio Limit, at low and high electron densities is

$$R = \begin{cases} 1 + 2\frac{\gamma_v}{\gamma_{UV}} & N_e \to 0 \\ 2\frac{\gamma_v}{\gamma_{UV}} & N_e \to \infty \end{cases} \tag{4.90}$$

With no coherence excited by electron collisions, the ratio is given by

$$R = \frac{\gamma_v(\gamma_{UV} + 2(\gamma_v + r_v))}{\gamma_{UV}(\gamma_v + r_v)} \tag{4.91}$$

H. Discussion

So far we discussed the suppression of spontaneous decay on the visible transition. This suppression is due to the two-photon coherence induced by the interference of collisional processes along two overlapping optical transitions $|a\rangle - |c\rangle$ and $|b - |c\rangle$. In order to quantify the degree of the suppression we introduced the branching ratio as the ratio of total spectral-line intensities for the two transitions. Here, one transition is the visible transition (actually, simultaneously two transitions) of interest and the other transition is the reference ultraviolet transition. This branching ratio calculated for the case of maximal two-photon coherence, see Eq. (4.65), is compared to the branching ratio evaluated for the case of no coherence, see Eq. (4.71). The degree of the coherence-induced suppression can be deduced as the ratio of these two branching ratios, i.e.

$$R = \gamma_{UV} \left(\frac{4}{r_e} + \frac{1}{r_{vis}} \right) \tag{4.92}$$

The formula is valid as long as inequality (4.34) holds. The faster the collision rates the stronger the interference of the optical channels and the larger the degree of the suppression. Physically, the suppression of the spontaneous decay on the visible transition is associated with putting most atoms in the non-emitting dark state, while only a small fraction of the atoms left in the bright state participates in the emission, as comparison of populations given by formulas (35) and (36) illustrates.

The important message of this study is the demonstration of the possibility of coherent effects in plasmas, where the coherence is induced by the interference of incoherent processes. Here the collisions of free electrons with ions represent these incoherent processes, and they indeed happen rather frequently for concentrations as high as $10^{18} cm^{-3}$. When they dominate over relevant decay rates, the two-photon coherence becomes of substantial value that leads to efficient suppression of the spon-

taneous emission on the visible transition. This suppression was registered experimentally and reported by Chung, Lemaire, and Suckewer in Ref. [81]. Simultaneously, no suppression was registered for the spontaneous radiation on the ultra-violet transition. So, the effect shows up when these two emissions are compared in terms of the branching ratio. With our theoretical model we can reveal and explain these features. Moreover, we are able to explain sensitive dependence of the degree of suppression on concentration of free electrons. It is interesting that the dependence on the concentration only appears due to the collision-induced coherence and disappears in the absence of the coherence, as comparing Eqs. (4.65) and (4.71) shows.

Motivated by the comparison in our study with the experiment, we draw attention mainly to the role of quantum coherence in suppression of the spontaneous decay. An interesting question is whether this coherence can cause the opposite effect, namely the enhancement of the spontaneous emission. The answer is positive, provided we modify a little our model. Let us eliminate the pumping rate r_e via auxiliary upper state $|e\rangle$, while keeping other pumping and decay rates intact. Effectively, the five-level model reduces now to four levels. Equations (4.31)-(4.33) have simple solutions. They become even simpler under our main assumption that the pumping rate r_{vis} dominates over the other rates. The population of the dark state decays to zero while the bright state is equally populated as the lower state $|c\rangle$:

$$\rho_{BB} \approx \rho_{cc} \tag{4.93}$$

Since the dark-bright coherence is as small as $-(\gamma_{UV}/4r_{vis})\rho_{BB}$, the population of $|a\rangle$ state is given by

$$\rho_{aa} \approx \frac{1}{2}\rho_{BB} \approx \frac{1}{2}\rho_{cc} \tag{4.94}$$

Taking the ratio as in Eq. (4.63), we formulate the branching ratio for the visible

and ultraviolet transitions:

$$R = 4\frac{\gamma_{vis}}{\gamma_{UV}} \tag{4.95}$$

We get twice as strong emission as in the case with no coherence, compared to Eq. (4.71). This doubling is the largest that we can get as the enhancement factor for the rate of spontaneous emission.

Of course, this case with zero value of r_e is not realizable in plasmas where all pumping rates scale with energy according to the Boltzman distribution (4.68) and cannot be controlled from outside. However, this case demonstrates another facet of the quantum coherence. Here, as in the case of suppression, the coherence is again of large (maximal possible) value, but now with opposite sign: $\rho_{ab} \approx \frac{1}{2}\rho_{cc}$. Physically, all populations of upper states are concentrated in the emitting bright state $|B\rangle$, while the non-emitting dark state is empty. Therefore, the emission becomes as strong as it can be.

In conclusion, we suggested the model for demonstrating quantum interference effects in multi-level systems and following [81] proposed the branching ratio defined according to formula (4.2) as the measure of suppression/enhancement of spontaneous emission in multi-level configurations. We applied the scheme to the interpretation of experimental results reported in Ref. [81] and studied in detail the effect of suppression of spontaneous emission on the visible transition as opposed to the absence of the suppression effect on the ultraviolet transition.

In particular, we revealed the characteristic dependence of the branching ratio on the concentration of free electrons: an order of magnitude increase in the concentration corresponded to one order of magnitude decrease in the branching ratio. To our knowledge, this interpretation is the first attempt in explaining experimental results in high-density plasmas from the viewpoint of quantum interference. More experi-

ments and more elaborated theories are needed to conclude on the role of quantum coherence and interference in such manifestly incoherent media as plasmas.

CHAPTER V

FANO INTERFERENCE IN PHOTOVOLTAICS

A. Introduction

In this work we have studied the effect of Fano interference on the efficiency of solar cell. This interference is induced by two spontaneous decays from discrete doublet ground states to an identical continuum in a three-level system. This system is based on a single-mode cavity pn-junction photo-cell irradiated by monochromatic light preliminarily selected out of the solar spectrum. In this model, as in previous works [54, 57], we neglect all the losses due to crystal vibrations that arise from the excess of the photon energy over the band-gap, the reflection losses, and the contacts and extraction losses. Here we are mainly focused on the radiative recombination losses.

The organization of this chapter is as follows. In section II we discuss the theoretical model of the three-level system, the dynamical evolution of the system, and the probability of absorption and emission. In section III we simulate the effect of the fano interference between the decay channels on the probability of absorption and emission. In section IV we show some analytical analysis of the fano interference in both the probability amplitude and the density matrix approaches. Finally in section V we summarize our results.

B. Theoretical model

An interesting example of Fano-like coupling is the three-level system as shown in Fig.22, where the effects of coherence play a major role. This scheme is developed from previous intersubband double quantum well structure [88]. Consider a ground state doublet $|v_{1,2}\rangle$ and an excited state $|c\rangle$ coherently driven by laser field with the

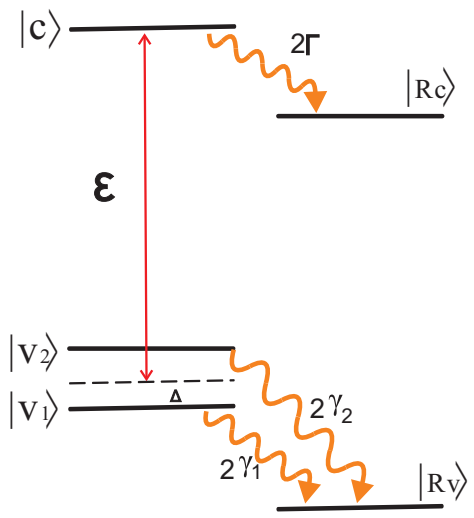

Fig. 22. Scheme of the three-level system with doublet in the ground state. $\mathcal{E}$ is the external applied weak electric field. 2Γ and $2\gamma_{1,2}$ are spontaneous decay rates from eigenstates to continuums.

central frequency ν so that the energies of the state $|v_{1,2}\rangle$ are related to $|c\rangle$ as $\hbar(\nu \pm \Delta)$, where Δ is now frequency detuning, not the tunneling in [88]. Here the ground state doublet decays to an identical continuum (we consider this continuum as a reservoir state R_v) with rate $2\gamma_{1,2}$, and the excited state $|c\rangle$ decays to continuum (reservoir state R_c) with rate 2Γ.

To get the dynamical evolution of this system, we can use both the probability amplitude method and the density matrix method. In the probability amplitude method, we can write the state vector as

$$|\Psi\rangle = v_1|v_1\rangle + v_2|v_2\rangle + c|c\rangle \tag{5.1}$$

The dynamical equations of amplitude can be derived with the Weisskopf-Wigner approximation, which are also given in [88] for intersubband double quantum well structure by simply adding the decay term of 2Γ from the excited state $|c\rangle$ to the

reservoir $|R_c\rangle$,

$$\dot{v}_2 = -(\gamma_2 + i\Delta)v_2 - p\sqrt{\gamma_1\gamma_2}v_1 - i\Omega_2 c \tag{5.2}$$

$$\dot{v}_1 = -(\gamma_1 - i\Delta)v_1 - p\sqrt{\gamma_1\gamma_2}v_2 - i\Omega_1 c, \tag{5.3}$$

$$\dot{c} = -i\Omega_2 v_2 - i\Omega_1 v_1 - \Gamma c, \tag{5.4}$$

where $\Omega_1 = \wp_{cv_1}\varepsilon/\hbar$, $\Omega_2 = \wp_{cv_2}\varepsilon/\hbar$ are the Rabi frequencies of the applied field. $\wp_{cv_1}(\wp_{cv_2})$ is the dipole moment of the transition $|c\rangle \leftrightarrow |v_1\rangle$ ($|c\rangle \leftrightarrow |v_2\rangle$), and $\mathcal{E}_0$ is the applied electric field. The terms containing the product of decay rates appear due to the interference introduced by the decay of the two optical transitions to the same state. This is the so called Fano interference, which couples the doublet states. In order to measure the strength of interference, we introduce the p factor, which is the normalized scalar product of the corresponding dipole moments:

$$p = \frac{\wp_{cv_1} \cdot \wp_{cv_2}}{|\wp_{cv_1}\wp_{cv_2}|} \tag{5.5}$$

According to its definition, the alignment factor takes the value 1 for parallel dipole moments and -1 for antiparallel dipole moments, which correspond to the maximal coherence. Zero(0) is for the orthogonal situation, which gives no interference. Intermediate values on the $[-1, 1]$ segment are also possible. The extremes of maximal and minimal coherences deserve special attention.

Similarly, we can derive the dynamical equations in the format of density matrix. In the rotating-wave approximation, the semiclassical time-dependent interaction Hamiltonian that describes the atom-laser coupling for this Λ system is given by

$$H_{int} = -\hbar\left(\Omega_1 e^{-i\Delta t}|c\rangle\langle v_1| + \Omega_2 e^{i\Delta t}|c\rangle\langle v_2| + H.C.\right) \tag{5.6}$$

The time evolution of the density matrix is given by the master equation

$$\dot{\rho} = -\frac{i}{\hbar}[H_{int}, \rho] + L\rho; \tag{5.7}$$

where $L\rho = L_1\rho + L_2\rho$ describes spontaneous emission terms. It is known that the spontaneous decay rate between two levels $|1\rangle$,$|2\rangle$is given by

$$\gamma = \frac{1}{4\pi\epsilon_0}\frac{4\omega^3\wp_{12}^2}{3\hbar c^3} = \frac{\omega^3}{3\pi\hbar c^3\epsilon_0}\wp_{12}^2 \tag{5.8}$$

Let $\gamma' = \frac{\omega^3}{3\pi\hbar c^3\epsilon_0}$, then $\gamma = \gamma'\wp_{12}^2$, thus the relaxation terms become

$$\begin{aligned} L_1\rho = \; & - \; \gamma'[(\wp_{cv_1}\sigma_1^+ + \wp_{cv_2}\sigma_2^+)(\wp_{cv_1}\sigma_1 + \wp_{cv_2}\sigma_2)\rho & (5.9)\\ & + \; \rho(\wp_{cv_1}\sigma_1^+ + \wp_{cv_2}\sigma_2^+)(\wp_{cv_1}\sigma_1 + \wp_{cv_2}\sigma_2) & (5.10)\\ & - \; 2(\wp_{cv_1}\sigma_1 + \wp_{cv_2}\sigma_2)\rho(\wp_{cv_1}\sigma_1^+ + \wp_{cv_2}\sigma_2^+)]; & (5.11) \end{aligned}$$

$$L_2\rho = -\Gamma[\sigma_3^+\sigma_3\rho + \rho\sigma_3^+\sigma_3 - 2\sigma_3\rho\sigma_3^+]; \tag{5.12}$$

Here $\sigma_1^+ = |v_1\rangle\langle R_v|$, $\sigma_2^+ = |v_2\rangle\langle R_v|$, and $\sigma_3^+ = |c\rangle\langle R_c|$ are the atomic transition operators. We have taken into consideration the interference introduced by the two decays from the doublet states to the same continuum.

On expanding Eq. (5.7) in the basis $|c\rangle, |v_1\rangle, |v_2\rangle, |R_c\rangle, |R_v\rangle$, and using the relaxation Equations(5.11-5.12), we get the dynamical evolution of the density matrix elements as,

$$\dot{\rho_{11}} = i\Omega_1^*\rho_{c1} - i\Omega_1\rho_{1c} - 2\gamma_1\rho_{11} - p\sqrt{\gamma_1\gamma_2}(\rho_{12} + \rho_{21}) \tag{5.13}$$

$$\dot{\rho_{22}} = i\Omega_2^*\rho_{c2} - i\Omega_2\rho_{2c} - 2\gamma_2\rho_{22} - p\sqrt{\gamma_1\gamma_2}(\rho_{12} + \rho_{21}) \tag{5.14}$$

$$\dot{\rho_{44}} = 2\Gamma\rho_{33} \tag{5.15}$$

$$\dot{\rho_{55}} = 2\gamma_1\rho_{11} + 2\gamma_2\rho_{22} + 2p\sqrt{\gamma_1\gamma_2}(\rho_{12} + \rho_{21}) \tag{5.16}$$

and the non-diagonal terms

$$\dot{\rho_{12}} = i\Omega_1^*\rho_{32} - i\Omega_2\rho_{13} - p\sqrt{\gamma_1\gamma_2}(\rho_{11} + \rho_{22}) - \Gamma_{12}\rho_{12} \tag{5.17}$$

$$\dot{\rho_{13}} = i\Omega_1^*(\rho_{33} - \rho_{11}) - i\Omega_2^*\rho_{12} - p\sqrt{\gamma_1\gamma_2}\rho_{23} - \Gamma_{13}\rho_{13} \tag{5.18}$$

$$\dot{\rho_{23}} = i\Omega_2^*(\rho_{33} - \rho_{22}) - i\Omega_1^*\rho_{21} - p\sqrt{\gamma_1\gamma_2}\rho_{13} - \Gamma_{23}\rho_{23} \tag{5.19}$$

where

$$\Gamma_{12} = \gamma_1 + \gamma_2 + 2i\Delta \tag{5.20}$$

$$\Gamma_{1c} = \Gamma + \gamma_1 + i\Delta \tag{5.21}$$

$$\Gamma_{2c} = \Gamma + \gamma_2 - i\Delta \tag{5.22}$$

are complex dephasing. Here we already exploit the norm preserving condition ($||\rho|| = 1$) of a density matrix for a closed system.

Defining the probability of emission as a sum of the population in the levels v_1, v_2 and R_v for the system in Fig. 22:

$$P_{\text{emiss}}(t) = 1 - \rho_{cc}(t) - \rho_{R_cR_c}(t), \tag{5.23}$$

with initial conditions $v_{1,2}(0) = 0$, $c(0) = 1$ and taking into account the evolution of level R_c: $\dot{\rho}_{R_cR_c}(t) = 2\Gamma\rho_{cc}(t)$, the probability of emission is:

$$P_{\text{emiss}}(t) = 1 - \rho_{cc}(t) - 2\Gamma\int_0^t \rho_{cc}(t')dt' \tag{5.24}$$

Similarly the probability of absorption is given by

$$P_{\text{abs}}(t) = \rho_{cc}(t) + \rho_{R_cR_c}(t) = \rho_{cc}(t) + 2\Gamma\int_0^t \rho_{cc}(t')dt' \tag{5.25}$$

These are all the formulas we will exploit to investigate this photovoltaics system.

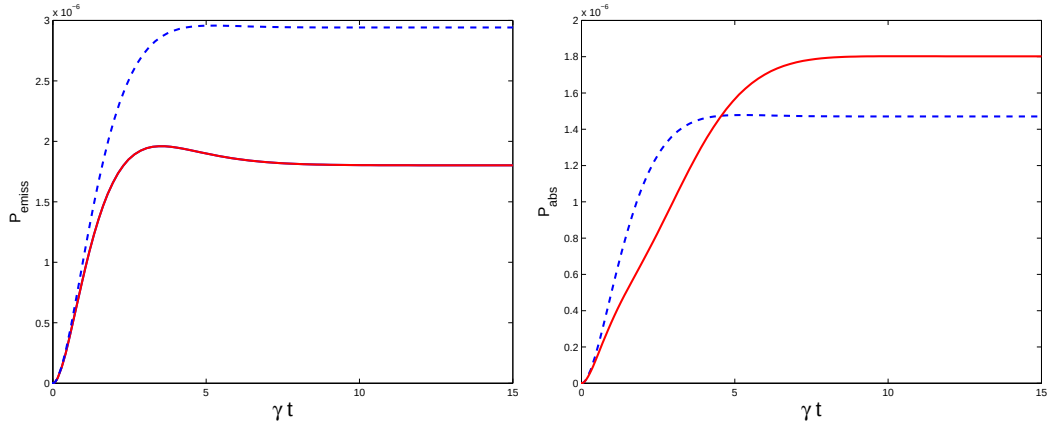

Fig. 23. Time dependence of probability of emission and absorption. $p = 1$ (solid red), $p = 0$ (dashed blue) with $\Omega_1 = \Omega_2 = 0.001, \Delta = 0.6, \Gamma = 1$, and $\gamma = 1$.

C. Numerical simulation

Fig. 23 shows the dependence of probability of emission and absorption on time with or without Fano interference. The red solid curves correspond to the maximal coherence with $p = 1$ and the blue dashed curves correspond to no coherence with $p = 0$. The parameters we are using are Rabi frequency $\Omega_1 = \Omega_2 = 0.001$, detuning $\Delta = 0.6$, and the spontaneous decay rate are $\Gamma = \gamma = 1$.

It is found that the effect of the Fano interference are apparent. We will take the steady states as an example. With $p = 0$, the probability of absorption is 1.47×10^{-6}, and the probability of emission is 2.94×10^{-6}. With $p = 1$, the probability of absorption is 1.8×10^{-6} and the probability of emission is 1.8×10^{-6}. Due to this fano interference, we get a nearly 22% increase in absorption and a 38% decrease in emission, which agrees with our theory that the balance between absorption and emission has been broken by the coherence induced by the spontaneous decays. It provides a possible method to significantly enhance the power generated by photo-cell.

Of course, we should also expect that the detuning also has effect on the probability of emission and absorption. Fig. 24 shows the same plots as shown in Fig. 23

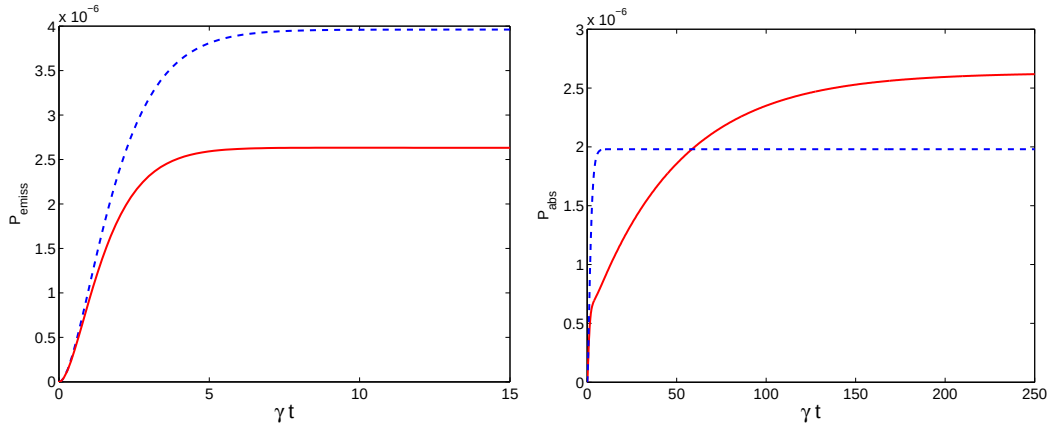

Fig. 24. Time dependence of probability of emission and absorption. $p = 1$ (solid red), $p = 0$ (dashed blue) with $\Omega_1 = \Omega_2 = 0.001, \Delta = 0.1, \Gamma = 1$, and $\gamma = 1$.

but with a smaller detuning $\Delta = 0.1$. We can see that under the same conditions, the probabilities of both emission and absorption increase with this smaller detuning. The interference plays a similar role, giving an increasing in absorption by 30% and a decrease in emission by 34%, which is very close to the situation with larger detuning.

D. Analytical analysis

To simplify the calculation, we will consider the special case where $\gamma_1 = \gamma_2 = \gamma$.

1. Probability amplitude approach

The two extremes of maximal and minimal coherences have special properties. We will only consider these two situations in our analysis. For the maximum coherence, we have $p = 1$, the dynamical Eqs.(5.2-5.4) become

$$\dot{v}_2 = -(\gamma + i\Delta)v_2 - \gamma v_1 - i\Omega_2 c \tag{5.26}$$

$$\dot{v}_1 = -(\gamma - i\Delta)v_1 - \gamma v_2 - i\Omega_1 c \tag{5.27}$$

$$\dot{c} = -i\Omega_2 v_2 - i\Omega_1 v_1 - \Gamma c, \tag{5.28}$$

Writing Eqs. (5.26-5.28) in matrix form, we obtain

$$\frac{d}{d\tau}\begin{pmatrix} v_2 \\ v_1 \\ c \end{pmatrix} = -V_f \begin{pmatrix} v_2 \\ v_1 \\ c \end{pmatrix} - iV_p \begin{pmatrix} v_2 \\ v_1 \\ c \end{pmatrix}, \tag{5.29}$$

where $\tau = \gamma t$, and the Fano decay matrix is defined by

$$V_f = \begin{pmatrix} 1+i\tilde{\Delta} & 1 & 0 \\ 1 & 1-i\tilde{\Delta} & 0 \\ 0 & 0 & \tilde{\Gamma} \end{pmatrix}, \tag{5.30}$$

and probe-field interaction is given by

$$V_p = \begin{pmatrix} 0 & 0 & \tilde{\Omega}_2 \\ 0 & 0 & \tilde{\Omega}_1 \\ \tilde{\Omega}_2 & \tilde{\Omega}_1 & 0 \end{pmatrix}, \tag{5.31}$$

with $\tilde{\Delta} = \frac{\Delta}{\gamma}$ and $\tilde{\Omega}_{1,2} = \frac{\Omega_{1,2}}{\gamma}$, $\tilde{\Gamma} = \frac{\Gamma}{\gamma}$. It is intuitive to introduce a dressed basis in which the Fano coupling is transformed away. We proceed from the bare basis via the U, U^{-1} matrices of diagonalization.

$$U^{-1} = \frac{1}{\sqrt{2}}\begin{pmatrix} 1 & 1 & 0 \\ x-i\tilde{\Delta} & -x-i\tilde{\Delta} & 0 \\ 0 & 0 & \sqrt{2} \end{pmatrix}, U = \frac{1}{\sqrt{2}x}\begin{pmatrix} x+i\tilde{\Delta} & 1 & 0 \\ x-i\tilde{\Delta} & -1 & 0 \\ 0 & 0 & \sqrt{2}x \end{pmatrix}, \tag{5.32}$$

Here $x = \sqrt{1-\tilde{\Delta}^2}$. so that the transformed state vector is defined by

$$U\begin{pmatrix} v_2 \\ v_1 \\ c \end{pmatrix} = \begin{pmatrix} A_+ \\ A_- \\ B \end{pmatrix}, \tag{5.33}$$

which implies

$$\begin{pmatrix} \dot{A}_+ \\ \dot{A}_- \\ \dot{B} \end{pmatrix} = -W_p \begin{pmatrix} A_+ \\ A_- \\ B \end{pmatrix} - iW_f \begin{pmatrix} A_+ \\ A_- \\ B \end{pmatrix}, \tag{5.34}$$

in which the diagonal operator is

$$W_f = UV_fU^{-1} \begin{pmatrix} 1+x & 0 & 0 \\ 0 & 1-x & 0 \\ 0 & 0 & \tilde{\Gamma} \end{pmatrix}, \tag{5.35}$$

and the transformed interaction potential is

$$W_p = UV_pU^{-1} = \frac{1}{\sqrt{2}} \begin{pmatrix} 0 & 0 & [\tilde{\Omega}_2(x+i\tilde{\Delta}) + \tilde{\Omega}_1]/x \\ 0 & 0 & [\tilde{\Omega}_2(x-i\tilde{\Delta}) - \tilde{\Omega}_1]/x \\ \tilde{\Omega}_2 + \tilde{\Omega}_1(x-i\tilde{\Delta}) & \tilde{\Omega}_2 - \tilde{\Omega}_1(x+i\tilde{\Delta}) & 0 \end{pmatrix}. \tag{5.36}$$

The equations of motion in terms of $A_\pm$ and B are then found to be

$$\frac{dA_+}{d\tau} = -(1+x)A_+ - \frac{i}{\sqrt{2}x}[\tilde{\Omega}_2(x+i\tilde{\Delta}) + \tilde{\Omega}_1]B, \tag{5.37}$$

$$\frac{dA_-}{d\tau} = -(1-x)A_- - \frac{i}{\sqrt{2}x}[\tilde{\Omega}_2(x-i\tilde{\Delta}) - \tilde{\Omega}_1]B, \tag{5.38}$$

$$\frac{dB}{d\tau} = -\frac{i}{\sqrt{2}}[\tilde{\Omega}_2 + \tilde{\Omega}_1(x-i\tilde{\Delta})]A_+ - \frac{i}{\sqrt{2}}[\tilde{\Omega}_2 - \tilde{\Omega}_1(x+i\tilde{\Delta})]A_- - \tilde{\Gamma}B, \tag{5.39}$$

Note that the transformed interaction matrix in Eq. (5.34) is not symmetric,i.e., it is non-Hermitian, thus the absorption-emission balance is broken.

From Eqs.(5.37-5.39), we can derive the analytical solutions of probability amplitude in the dressed states. To find the corresponding probability amplitude for emission, we take the initial condition as $B(0) = 1$ and $A_\pm(0) = 0$, and we assume the Rabi frequency of the driving fields $\Omega_{1,2}$ are weak enough so that we can apply

the perturbation method. The first order approximation of B is pure exponential function $B^{(0)} \cong e^{-\tilde{\Gamma}\tau}$. Compared to numerical simulations, this equation only works well for a short time in the beginning . A higher order approximation is needed. Replacing B in both Eqs.(5.37-5.38) with $B^{(0)}$, we get

$$\begin{aligned}\frac{dA_+^{(1)}}{d\tau} &= -(1+x)A_+^{(1)} - \frac{i}{\sqrt{2}x}[\tilde{\Omega}_2(x+i\tilde{\Delta}) + \tilde{\Omega}_1]e^{-\tilde{\Gamma}\tau} \\ \frac{dA_-^{(1)}}{d\tau} &= -(1-x)A_-^{(1)} - \frac{i}{\sqrt{2}x}[\tilde{\Omega}_2(x-i\tilde{\Delta}) - \tilde{\Omega}_1]e^{-\tilde{\Gamma}\tau}\end{aligned} \tag{5.40}$$

which gives the $A_\pm$

$$\begin{aligned}A_\pm^{(1)} &\cong -\frac{i}{\sqrt{2}x}[\tilde{\Omega}_2(x\pm i\tilde{\Delta}) \pm \tilde{\Omega}_1]\int_0^t e^{-(1\pm x-\tilde{\Gamma}\tau)(t-t')}dt' \\ &= -i\frac{e^{-\tilde{\Gamma}\tau} - e^{-(1\pm x)t}}{\sqrt{2}x(1\pm x-\tilde{\Gamma}\tau)}[\tilde{\Omega}_2(x\pm i\tilde{\Delta}) \pm \tilde{\Omega}_1],\end{aligned} \tag{5.41}$$

Substituting Eq. 5.41 into Eq.5.39, we get the next order of B, which is

$$B^{(1)} = (a_0\tau - a_1 - a_2 + 1)e^{-\tilde{\Gamma}\tau} + a_1 e^{-(1+x)\tau} + a_2 e^{-(1-x)\tau} \tag{5.42}$$

where

$$a_0 = \frac{[\tilde{\Omega}_2 + \tilde{\Omega}_1(x-i\tilde{\Delta})][\tilde{\Omega}_2(x+i\tilde{\Delta}) + \tilde{\Omega}_1]}{1+x-\tilde{\Gamma}} \tag{5.43}$$

$$+ \frac{[\tilde{\Omega}_2 - \tilde{\Omega}_1(x+i\tilde{\Delta})][\tilde{\Omega}_2(x-i\tilde{\Delta}) - \tilde{\Omega}_1]}{1-x-\tilde{\Gamma}} \tag{5.44}$$

$$a_1 = \frac{[\tilde{\Omega}_2 + \tilde{\Omega}_1(x-i\tilde{\Delta})][\tilde{\Omega}_2(x+i\tilde{\Delta}) + \tilde{\Omega}_1]}{(1+x-\tilde{\Gamma})^2} \tag{5.45}$$

$$a_2 = \frac{[\tilde{\Omega}_2 - \tilde{\Omega}_1(x+i\tilde{\Delta})][\tilde{\Omega}_2(x-i\tilde{\Delta}) - \tilde{\Omega}_1]}{(1+x-\tilde{\Gamma})^2} \tag{5.46}$$

Similarly, we can get the probability amplitude for absorption. There is no population in the ground state and the initial condition is $c(0) = 0$, $v_1 = 1$ or $v_2 = 1$. Thus we have $B(0) = 0$, and $A\pm$ can be derived by the linear transformation relations

between bar states and dressed states

$$A_{\pm} = \frac{1}{\sqrt{2}x}[v_2(x \pm i\tilde{\Delta}) \pm v_1] \tag{5.47}$$

For $v_1 = 1$, $A_{\pm} = \pm\frac{1}{\sqrt{2}x}$. In the situation of weak field, we have the first order approximation of $A_{\pm}$,

$$A_{\pm}^{(0)} = \pm\frac{1}{\sqrt{2}x}e^{-(1\pm x)} \tag{5.48}$$

Substituting Eq. 5.48 into Eq. 5.39, the next order of B is

$$B^{(1)} = (b_+ - b_-)e^{-\tilde{\Gamma}\tau} - b_+e^{-(1+x)\tau} + b_-e^{-(1-x)\tau} \tag{5.49}$$

where

$$b_{\pm} = -i\frac{[\tilde{\Omega}_2 \pm \tilde{\Omega}_1(x \mp i\tilde{\Delta})]}{2x(1 \pm x - \tilde{\Gamma})} \tag{5.50}$$

For $v_2 = 1$, we have $A_{\pm} = \pm\frac{x \pm i\tilde{\Delta}}{\sqrt{2}x}$. Compared with the situation $v_1 = 1$, there is only a time-independent coefficient difference. We can directly write it down as B

$$B^{(1)} = (b_+(x+i\tilde{\Delta}) - b_-(x-i\tilde{\Delta}))e^{-\tilde{\Gamma}\tau} + b_+e^{-(1+x)\tau}(x+i\tilde{\Delta}) + b_-e^{-(1-x)\tau}(x-i\tilde{\Delta}) \tag{5.51}$$

where $b_{\pm}$ are the same as defined for $v_1 = 1$.

For the situation without coherence, or $p = 0$, the calculation is straightforward. No dressed states are need. Eqs.(5.2-5.4) become

$$\dot{v}_2 = -(\gamma + i\Delta)v_2 - i\Omega_2 c, \tag{5.52}$$

$$\dot{v}_1 = -(\gamma - i\Delta)v_1 - i\Omega_1 c, \tag{5.53}$$

$$\dot{c} = -i\Omega_2 v_2 - i\Omega_1 v_1 - \Gamma c, \tag{5.54}$$

For emission, we have the same initial condition of $c(0) = 1$, $v_{1,2}(0) = 0$. Thus

the first order approximation of c is

$$c^{(0)} = e^{-\tilde{\Gamma}t} \tag{5.55}$$

and $v_{1,2}$ are given by

$$\begin{aligned} v_1^{(0)} &= \frac{i\tilde{\Omega}_1}{\tilde{\Gamma} - \tilde{\Gamma_1}}(e^{-\tilde{\Gamma}t} - e^{-\tilde{\Gamma_1}t}) \\ v_2^{(0)} &= \frac{i\tilde{\Omega}_2}{\tilde{\Gamma} - \tilde{\Gamma_2}}(e^{-\tilde{\Gamma}t} - e^{-\tilde{\Gamma_2}t}) \end{aligned} \tag{5.56}$$

where

$$\tilde{\Gamma_1} = 1 - i\tilde{\Delta} \tag{5.57}$$

$$\tilde{\Gamma_2} = 1 + i\tilde{\Delta} \tag{5.58}$$

Substituting Eq. 5.56 into Eqs. (5.54), we get the next order of probability amplitude,

$$c^{(1)} = (a_0 t - a_1 - a_2 + 1)e^{-\tilde{\Gamma}t} + a_1 e^{-\tilde{\Gamma_1}t} + a_2 e^{-\tilde{\Gamma_2}t} \tag{5.59}$$

where

$$a_0 = (\frac{\tilde{\Omega_1}^2}{\tilde{\Gamma} - \tilde{\Gamma_1}} + \frac{\tilde{\Omega_2}^2}{\tilde{\Gamma} - \tilde{\Gamma_2}});\ a_1 = \frac{\tilde{\Omega_1}^2}{(\tilde{\Gamma} - \tilde{\Gamma_1})^2};\ a_2 = \frac{\tilde{\Omega_2}^2}{(\tilde{\Gamma} - \tilde{\Gamma_2})^2} \tag{5.60}$$

At large time $\tau \gg 1, 1/\tilde{\Gamma}$ and with weak field approximation, by applying Eq.5.24, we can get the probability of emission

$$P_{\text{emiss}} \simeq \frac{(4\Delta^2(3\Gamma - 1) + (\Gamma^2 - 1)(3\Gamma + 1))(4\Omega_1^2 + 4\Omega_2^2)}{(4\Delta^2 + 1)^2\Gamma + 2(4\Delta^2 - 1)\Gamma^3 + \Gamma^5} \tag{5.61}$$

For absorption, we only show the initial condition $v_1(0) = 1$, $c(0) = 0$ as an example. Following the same process, we get

$$v_1^{(0)} = e^{-\Gamma_1 t} \tag{5.62}$$

$$c^{(0)} = \frac{i\Omega_1}{\Gamma_1 - \Gamma}\left(e^{-\Gamma_1 t} - e^{-\Gamma t}\right) \tag{5.63}$$

$$v_2^{(0)} = \frac{\Omega_1 \Omega_2^*}{\Gamma_1 - \Gamma} \left(\frac{e^{-\Gamma t} - e^{-\Gamma_2 t}}{\Gamma_2 - \Gamma} + \frac{e^{-\Gamma_1 t} - e^{-\Gamma_2 t}}{\Gamma_1 - \Gamma_2} \right) \tag{5.64}$$

$$c^{(1)} = -ib_0 e^{-\Gamma t} - \frac{ib_1}{\Gamma - \Gamma_1}(e^{-\Gamma_1 t} - e^{-\Gamma t}) - \frac{ib_2}{\Gamma - \Gamma_2}(e^{-\Gamma_2 t} - e^{-\Gamma t}) \tag{5.65}$$

in which

$$b_0 = \frac{\Omega_1 |\Omega_2|^2}{(\Gamma_1 - \Gamma)(\Gamma_2 - \Gamma)} \tag{5.66}$$

$$b_1 = \Omega_1 \left(\frac{|\Omega_2|^2}{(\Gamma_1 - \Gamma)(\Gamma_1 - \Gamma_2)} + 1 \right) \tag{5.67}$$

$$b_2 = \frac{\Omega_1 |\Omega_2|^2}{(\Gamma_2 - \Gamma)(\Gamma_1 - \Gamma_2)} \tag{5.68}$$

By applying Eq.5.25, the probability of absorption is given by

$$\begin{aligned} P_{\text{abs}}(\tau|c) &= \rho_{cc}(\tau) + 2\tilde{\Gamma} \int_0^\tau \rho_{cc}(\tau') d\tau' \\ &\simeq \frac{4\Omega_1^2(1+\Gamma)}{4\Delta^2 + (\Gamma+1)^2}. \end{aligned} \tag{5.69}$$

2. Density matrix approach

It will be great to derive the analytical solution of probability of emission and absorption in the density element form. However, it has found to be too complex with the existence of coherence. Here, we will only take the simple situation without interference($p = 0$) as an example. The density matrix becomes

$$\dot{\rho_{11}} = i\Omega_1^* \rho_{c1} - i\Omega_1 \rho_{1c} - \gamma \rho_{11} \tag{5.70}$$

$$\dot{\rho_{22}} = i\Omega_2^* \rho_{c2} - i\Omega_2 \rho_{2c} - \gamma \rho_{22} \tag{5.71}$$

$$\dot{\rho_{cc}} + \dot{\rho_{Rc}} = -i\Omega_1(\rho_{c1} - \rho_{1c}) - i\Omega_2(\rho_{c2} - \rho_{2c}) \tag{5.72}$$

$$\dot{\rho_{12}} = i\Omega_1^* \rho_{c2} - i\Omega_2 \rho_{1c} - \Gamma_{12} \rho_{12} \tag{5.73}$$

$$\dot{\rho_{1c}} = i\Omega_1^*(\rho_{cc} - \rho_{11}) - i\Omega_2^* \rho_{12} - \Gamma_{1c} \rho_{1c} \tag{5.74}$$

$$\dot{\rho_{2c}} = i\Omega_2^*(\rho_{cc} - \rho_{22}) - i\Omega_1^* \rho_{21} - \Gamma_{2c} \rho_{2c} \tag{5.75}$$

Notice that Eq.(5.72) is already the time derivation of the core of probability of emission and absorption formulas. It is the key to solve this equations. With the initial condition of $\rho_{cc} = 1$, Eq.(5.74,5.75) will give us the same time evolution of ρ_{1c} and ρ_{2c}, thus

$$\rho_{1c} = \frac{i\Omega_1}{\Gamma_{13} - \gamma}(e^{-\gamma t} - e^{-\Gamma_{13} t}) \tag{5.76}$$

Integrating on both sides from zero to infinity, we get the probability of emission

$$P_{emiss} = \frac{4(\Omega_1^2 + \Omega_2^2)}{4\Delta^2 + \Gamma^2} \frac{(4\Delta^2 + \Gamma^2)\Gamma + \Gamma^2 - 4\Delta^2}{4\Delta^2 + (\Gamma + 1)^2} \tag{5.77}$$

For the absorption, we have $\rho_{11}(0) = 1$, substituting it into Eq. (5.70), we get $\rho_{11}(t) = e^{-\gamma t}$. From Eq. (5.74), we get

$$\rho_{1c} = \frac{i\Omega_1}{\gamma - \Gamma_{13}}(e^{-\gamma t} - e^{-\Gamma_{13} t}) \tag{5.78}$$

From the results of numerical simulations, we found that ρ_{2c} is always much smaller than ρ_{1c} with the approximation have have assumed. We can ignore the contribution by ρ_{2c}. Thus

$$\begin{aligned} \dot{\rho_{cc}} + \dot{\rho_{Rc}} &= -i\Omega_1(\rho_{c1} - \rho_{1c}) \\ &= \frac{\Omega_1^2}{\Delta^2 + \Gamma^2}(2\Gamma e^{-\gamma t} - e^{-(\Gamma+\gamma)t}(2\Gamma cos(\Delta t) + 2\Delta sin(\Delta t)) \end{aligned} \tag{5.79}$$

Integrating on both sides from zero to infinity again, we get

$$P_{abs} = \frac{4\Omega_1^2}{4\Delta^2 + \Gamma^2} \frac{(4\Delta^2 + \Gamma^2)\Gamma + \Gamma^2 - 4\Delta^2}{4\Delta^2 + (\Gamma + 1)^2} \tag{5.80}$$

To verify the analytical solutions, we can compare them with numerical results. Let's take the same parameters we have used in Fig.23 except that here we have $p = 0$. In the steady states, we have $P_{emiss} = 3.992 \times 10^{-6}$ for analytical solution and $P_{emiss} = 3.998 \times 10^{-6}$ for numerical solution, and $P_{abs} = 1.996 \times 10^{-6}$ for analytical solution and $P_{abs} = 1.999 \times 10^{-6}$ for numerical solution. Both sets match well, which

shows that these two analytical solutions are good enough to describe the emission and absorption dependence on the system parameters.

E. Conclusion

In this chapter, we studied the effect of the fano interference in a three-level system with reservoir. It is found that this interference can largely suppress the emission process and enhance the absorption process. Thus it can increase the probability of absorption and decrease of the probability of emission, and becomes possible to improve the efficiency of solar cell. This shows that the balance between emission and absorption for the original system has been broken. Under the weak field approximation, the analytical solutions of probability amplitude and density elements are derived. They matched well with numerical simulations.

CHAPTER VI

SUMMARY

In summary, we have studied the effect of coherent interference in light-matter interaction processes with several different systems.

We present a theoretical study of Electromagnetically Induced Transparency (EIT) with $0-\pi$ pulses and find that even on two-photon resonance the absorption of the $0-\pi$ pulses is significantly greater than that of the Gaussian pulses. This pulse shape effect on the efficiency of EIT is explained by the dark and bright states. The effect may find a possible application in developing an all-optical switch.

We suggest an approach that extends application of the stimulated Raman scattering to media with a lot of scattering. The stimulated Raman scattering has an advantage of relaxing phase-matching condition which is difficult or even impossible to meet under condition of strong scattering. This technique is compatible and can be applied to microscopy.

We develop a model for demonstrating quantum interference effects in multi-level systems and use the branching ratio as the measure of suppression of spontaneous emission in multi-level configurations. We apply the scheme to interpret the experimental results and reveal the characteristic dependence of the branching ratio on the concentration of free electrons.

Finally we study the effect of fano interference in a three-level system with reservoir. It is found that this interference can largely suppress the emission process and enhance the absorption process, and break the balance between emission and absorption. It can possibly be applied in improving the efficiency of solar cell. Under weak field approximation, the analytical solutions of probability amplitude and density elements are derived.

REFERENCES

[1] E. Arimondo, in Progress in Optics, edited by E. Wolf (Elsevier Science, Amsterdam, 1996), Vol. XXXV, p. 257.

[2] M. O. Scully and M. S. Zubairy, Quantum Optics (Cambridge University Press, Cambridge, England, 1997).

[3] S. E. Harris, Phys. Today **50**, 36 (1997).

[4] S. E. Harris, Phys. Rev. Lett. 70, 552 (1993).

[5] M. Fleischhauer, A. Imamoglu, and J. P. Marangos, Rev. Mod. Phys. **77**, 633 (2005).

[6] O. Kocharovskaya, and Y. I. Khanin, Sov. Phys. JETP **63**, 945 (1986).

[7] V.A. Sautenkov, Y.V. Rostovtsev, C. Y. Ye, G.R. Welch, O. Kocharovskaya, and M.O. Scully, Phys. Rev. A **71**, 063804 (2005).

[8] M. O. Scully, Phys. Rev. Lett. **67**, 1855 (1991); M. O. Scully and M. Fleischhauer, *ibid*, **69**, 1360 (1992); A. S. Zibrov *et. al. ibid* **76**, 3935 (1996).

[9] L.V. Hau, S.E. Harris, Z. Dutton, and C.H. Behroozi, Nature **397**, 594 (1999); C. Liu, Z. Dutton, C.H. Behroozi, and L.V. Hau, Nature **409**, 490 (2001).

[10] M.M. Kash, V.A. Sautenkov, A.S. Zibrov, L. Hollberg, G.R. Welch, M.D. Lukin, Y. Rostovtsev, E.S. Fry, and M.O. Scully, Phys. Rev. Lett. **82**, 5229 (1999). D. Budker, D.F. Kimball, S.M. Rochester, and V.V. Yashchuk, Phys. Rev. Lett. **83**, 1767 (1999).

[11] L.J. Wang, A. Kuzmich, and A. Dogariu, Nature (London) **406**, 277 (2000); A. Dogariu, A. Kuzmich, and L.J. Wang, Phys. Rev. A **63**, 053806 (2001).

[12] G. S. Agarwal, T. N. Dey, and S. Menon, Phys. Rev. A **64**, 053809 (2001).

[13] E.E. Mikhailov, V.A. Sautenkov, Y.V. Rostovtsev, and G.R. Welch, J. Opt. Soc. Am. B **21**, 425 (2004); Q. Sun, Y.V. Rostovtsev, J.P. Dowling, M.O. Scully, and M. S. Zubairy, Phys. Rev. A **72**, 031802 (2005).

[14] A. B. Matsko, Y. V. Rostovtsev, M. Fleischhauer, and M. O. Scully, Phys. Rev. Lett. **86**, 2006 (2001).

[15] Y.V. Rostovtsev, Z.-E. Sariyanni, and M.O. Scully, Phys. Rev. Lett. **97**, 113001 (2006).

[16] V. Sautenkov, Y.V. Rostovtsev and M.O. Scully, Phys. Rev. A**72**, 065801 (2005).

[17] H. Li,V. A. Sautenkov,Y. V. Rostovtsev,G. R. Welch,P. R. Hemmer, and M. O. Scully, Phys. Rev. A **80**, 023820 (2009)

[18] M. Fleischhauer and M.D. Lukin, Phys. Rev. Lett. **84**, 5094 (2000); Phys. Rev. A **65**, 022314 (2002); D.F. Phillips, A. Fleischhauer, A. Mair, R.L. Walsworth, and M.D. Lukin, Phys. Rev. Lett. **86**, 783 (2001).

[19] A. B. Matsko, Y. V. Rostovtsev, O. Kocharovskaya, A. S. Zibrov, and M. O. Scully, Phys. Rev. A **64**, 043809 (2001); C. Mewes and M. Fleischhauer, Phys. Rev. A **66**, 033820 (2002); T. N. Dey and G. S. Agarwal, Phys. Rev. A **67**, 033813 (2003).

[20] O. Kocharovskaya, Y. Rostovtsev, and M.O. Scully, Phys. Rev. Lett. **86**, 628 (2001).

[21] M. O. Scully, and M. Fleischhauer, Phys. Rev. Lett. **69**, 1360 (1992); M. Fleischhauer, and M. O. Scully, Phys. Rev. A **49**, 1973 (1994); V. A. Sautenkov, M. D. Lukin, C. J. Bednar, et al., Phys. Rev. A **62**, 023810 (2000); M. Fleischhauer, A. B. Matsko, and M. O. Scully, Phys. Rev. A **62**, 013808 (2000).

[22] D. Budker, W. Gawlik, D.F. Kimball, S.M. Rochester, V.V. Yashchuk, and A. Weis, Rev. Mod. Phys. **74**, 1153 (2002); D. Budker, and M. Romalis, Nature Phys. **3**, 227 (2007); A. Edelstein, J. Phys.-Cond. Mat. **19**, 165217 (2007).

[23] M. Kiffner, and T. N. Dey, Phys. Rev. A**79**, 023829 (2009).

[24] A. Andre, M.D. Eisaman, R.L. Walsworth, A. S. Zibrov, and M.D. Lukin, J. Phys. B: At. Mol. Opt. Phys. **38**, 589 (2005).

[25] M. Mucke, E. Figueroa, J. Bochmann, C. Hahn, K. Murr, S. Ritter, C. J. Villas-Boas, and G. Rempe, Nature **465**, 755-758, (2010).

[26] S.E. Harris, and Y. Yamamoto, Phys. Rev. Lett. **81**, 3611 (1998).

[27] J. Clarke, H. Chen, and W. A. V. Wijngaarden, Applied Optics **40**, 2047 (2001).

[28] B. S. Ham, J. of modern optics **49**, 2477 (2002).

[29] P. Ginzburg and M. Orenstein, Integrated Photonics Research and Applications/Nanophotonics, Technical Digest (CD) (Optical Society of America, 2006), paper IMC3.

[30] C. Y. Ye, V. A. Sautenkov, Y. V. Rostovtsev, and M. O. Scully, Opt. Lett. **28**, 2213 (2003).

[31] S. E. Harris, and Y. Yamamoto, Phys. Rev. Lett. **81**, 3611 (1998).

[32] M. D. Lukin, P. R. Hemmer, and M. O. Scully, Adv. in At. Mol. Opt. Phys. **42**, 347 (2000).

[33] N. G. Kalugin, and Y. Rostovtsev, Opt. Lett. **31**, 969 (2006).

[34] E. Kuznetsova, Y. Rostovtsev, N.G. Kalugin, R. Kolesov, O. Kocharovskaya, and Marlan O. Scully, Phys. Rev. A **74**, 023819 (2006).

[35] J. B. Qi and A. M. Lyyra, Phys. Rev. A **73**, 043810 (2006); L. Li, P. Qi, A. Lazoudis, E. Ahmed, and A. M. Lyyra, Chem. Phys. Lett. **403**, 262 (2005).

[36] H. Li, H. Chen, M. A. Gubin, Y. V. Rostovtsev, V. A. Sautenkova, and M. O. Scully, Laser Physics **20**, 1725 (2011).

[37] K. Ichimura, K. Yamamoto, and N. Gemma, Phys. Rev. A **58**, 4116(1998).

[38] Y. Zhao, C. Wu, B. S. Ham, M. K. Kim, and E. Awad, Phys. Rev. Lett. **79**, 641 (1997).

[39] B. S. Ham, M. S. Shahriar, and P. R. Hemmer, Opt. Lett. **22**, 1138 (1997)

[40] N. Liu, T. Weiss, M. Mesch, L. Langguth, U. Eigenthaler, M. Hirscher, C. Snnichsen, and H. Giessen, Nano Lett. **10**, 1103 (2010)

[41] V. A. Fedotov, M. Rose, S. L. Prosvirnin, N. Papasimakis, and N. I. Zheludev, Phys. Rev. Lett. **99**, 147401 (2007) N. Papasimakis, V. A. Fedotov, and N. I. Zheludev, Phys. Rev. Lett. **101**, 253903 (2008).

[42] S. Chiam, R. Singh, C. Rockstuhl, F. Lederer,W. Zhang, and A. A. Bettiol, Phys. Rev. B **80**, 153103 (2009).

[43] G. S. Agarwal and Sumei Huang, Phys. Rev. A **81**, 041803 (2010).

[44] M.O. Scully and M. S. Zubairy Quantum Optics, (Cambridge Press, London 1997)

[45] U. Fano, Phys. Rev. 124, 1866 (1961).

[46] G. S. Agarwal , Springer Tracts in Modern Physics: Quantum Optics (Springer-Verlag, Berlin, 1974).

[47] S. E. Harris, Phys. Rev. Lett. 62, 1033 (1989); M. O. Scully, S. -Y. Zhu, and A. Gavrielides, Phys. Rev. Lett. 62, 2813 (1989).

[48] O. Kocharovskaya, Phys. Rep. 219, 175 (1992).

[49] M. O. Scully, M. S. Zubairy, G. S. Agarwal, and H. Walther Science 299, 862 (2003).

[50] A. Ishizaki, and G . Fleming, PNAS 106, 17255 (2009).

[51] P. Wurfel, Physics of Solar Cells, (Wiley-VCH Verlag gmbH &Co., Weinheim, 2009).

[52] M. O. Scully, S.Y. Zhu, and A. Gavrielides, Phys. Rev. Lett. 62, 2813 (1989).

[53] S.E. Harris, Phys. Rev. Lett. 62, 1033 (1989).

[54] M. O. Scully, Phys. Rev. Lett. 104, 207701 (2010).

[55] U Fano, Phys. Rev. 124, 1866 (1961).

[56] M. O. Scully Coherent Control, Fano Interference, and Non-Hermitian Interactions, Workshop held in May, 1999 (Kluwer Academic Publishers, Norwell, MA, 2001).

[57] K. E. Dorfman, A. A. Svidzinsky, and M. O. Scully (unpublished) (2010)

[58] Y. Rostovtsev, I. Protsenko, H. Lee, and A. Javan, J. Mod. Opt. **49**, 2501 (2002); H. Lee, Y. Rostovtsev, C.J. Bednar, and A. Javan, Appl. Phys. B **76**, 33 (2003).

[59] L. Allen and J. H. Eberly, Optical Resonance and Two Level Atoms (Dover 1987).

[60] Z.E. Sariyanni, and Y. Rostovtsev, J. Mod. Opt. **51**, 2637 (2004).

[61] A. W. Brown, and M. Xiao, Opt. Lett. **30**, 699 (2005).

[62] Z. E. Sariyanni, D. Sun, and Y. Rostovtsev, to be published.

[63] M. C. Fischer, T. Ye, G. Yurtsever, A. Miller, M. Ciocca, W. Wagner, and W. S. Warren, Opt. Lett. **30**, 1551 (2005).

[64] Infrared and Raman Spectroscopy, Ed. B. Schrader (VCH, Tokyo, 1995).

[65] Femtochemistry and Femtobiology, Ed. M. M. Martin and J.T. Hynes (Eslvier, Tokyo, 2004).

[66] M. O. Scully, G. W. Kattawar, R. P. Lucht, et al., PNAS 99, 10994-11001 (2002).

[67] D. Pestov, M. Zhi, Z. E. Sariyanni, et al., PNAS 102, 14976-14981 (2005).

[68] M. C. Fischer, T. Ye, G. Yurtsever, A. Miller, M. Ciocca, W. Wagner, W. S. Warren, Opt. Lett. 30, 1551 (2005).

[69] Boyd, Nonlinear Optics.

[70] V. Weisskopf and E. Wigner, Z. Phys. 63, 54 (1930); 65, 18 (1931).

[71] S. Haroche and D. Kleppner, Phys. Today 44(1), 24 (1989).

[72] E. M. Purcell, Phys. Rev. 69, 681 (1946).

[73] P. Goy, J. M. Raimond, M. Gross, and S. Haroche, Phys. Rev. Lett. 50, 1903 (1983).

[74] D. Kleppner, Phys. Rev. Lett. 47, 233 (1981).

[75] D. A. Cardimona, M. G. Raymer, and C. R. Stroud, J. Phys. B 15, 55 (1982).

[76] L. M. Narducci, M. O. Scully, G.-L. Oppo, P. Ru, and J. R. Tredicce, Phys. Rev. A. 42, 1630 (1990).

[77] D. J. Gauthier, Y. Zhu, and T. W. Mossberg, Phys. Rev. Lett. 66, 2460 (1991).

[78] S. Y. Zhu and M. O. Scully, Phys. Rev. Lett. 76, 388 (1996).

[79] H. Lee, P. Polynkin, M. O. Scully, and S.-Y. Zhu, Phys. Rev. A 55, 4454 (1997).

[80] S. E. Harris, Phys. Rev. Lett. 62, 1033 (1989).

[81] Y. Chung, P. Lemaire, and S. Suckewer, Phys. Rev. Lett. 60, 1122 (1988).

[82] M. O. Scully and M. S. Zubairy, Quantum Optics, Cambridge University Press, Cambridge, 1997.

[83] M. Fleischhauer, C. H. Keitel, M. O. Scully, and C. Su, Opt. Commun. 87, 109-114 (1992).

[84] V. V. Kozlov, Yu. Rostovtsev, M. O. Scully, Phys. Rev. A74, 063829 (2006).

[85] L. M. Narducci, M. O. Scully, G.-L. Oppo, P. Ru, and J. R. Tredicce, Phys. Rev. A 42, 1630 (1990).

[86] Y. Chung, H. Hirose, and S. Suckewer, Phys. Rev. A 40, 7142 (1989).

[87] S. Glenzer, J. Musielok, and H.-J. Kunze, Phys. Rev. A 44, 1266 (1991).

[88] M. O. Scully, Advances in Multi-photon Processes and Spectroscopy, 14, pp 126-132 (1999)

VITA

Dong Sun

Physics Dept.

Texas A&M University 4242

College Station, Texas 77843-4242

Email Address: neiosun@tamu.edu

Education

Department of Physics, Texas A&M University, College Station, TX

Ph.D in Physics, Dec 2011

Department of Physics, University of Antwerp, Antwerp, Belgium

Advanced Master in Nanophysics, July 2006

Department of Physics, Zhejiang University, Hangzhou, China

B.S. in Physics, July 2005

The typist for this dissertation was Dong Sun.